The Pennsylvania State University

The Graduate School

College of Engineering

PRELIMINARY TESTING OF A 17.8-GHZ MICROWAVE ELECTROTHERMAL THRUSTER FOR SMALL SPACECRAFT

A Thesis in

Aerospace Engineering

by

Mikhail D Abaimov

Submitted in Partial Fulfillment
of the Requirements
for the Degree of

Master of Science

August 2015

The thesis of Mikhail D Abaimov was reviewed and approved* by the following:

Sven G. Bilén
Professor of Engineering Design, Electrical Engineering, and Aerospace Engineering
Thesis Advisor

Michael M. Micci
Professor of Aerospace Engineering and Director of Graduate Studies

George A. Lesieutre
Professor of Aerospace Engineering
Head of the Department of Aerospace Engineering

*Signatures are on file in the Graduate School

ABSTRACT

CubeSats are small satellites that conform to combinations of a standard 10×10×10 cm form factor. Currently, CubeSats have limited propulsion options because their restrictive size. This thesis details the design and initial testing of a CubeSat-scale microwave electrothermal thruster. The goal of this research was to lay the groundwork for future thruster designs that could be incorporated into CubeSat propulsion modules.

As part of this work, a prototype thruster head with a 17.8-GHz microwave resonant cavity was designed per dimensions determined from previous research and machined for experimentation. The candlestick antenna used in the design was optimized by varying its height above the bottom of the cavity and examining the reflected power measurements on a network analyzer. The rest of the testing setup was assembled for use with helium propellant. The power system consisted of a microwave signal generator driving a traveling-wave tube amplifier. Both cold and hot fire test results were performed. Cold flow maximum theoretical thrust was 4.77 mN, compared to a hot fire maximum theoretical thrust of 6.68 mN for the same flow rate of 2.15 mg/s. The maximum cold flow theoretical specific impulse was 225 seconds, and a maximum hot fire theoretical specific impulse of 349 seconds were achieved. The experimental setup was upgraded to allow use of anhydrous ammonia vapor as propellant. Ammonia testing was delayed, however, due to problems with the ammonia cylinder. Further work required to move the project forward is also discussed.

TABLE OF CONTENTS

LIST OF FIGURES

NOMENCLATURE

A_e	Nozzle exhaust area, m^2
A_z	Magnetic vector potential
A^*	Choked condition flow area, m^2
a	Resonant cavity radius, m
d	Distance between electrodes, m
c_p	Specific heat at constant pressure, J/kg·K
E	Electric field, V/m
E_t	Breakdown electric field, V/m
e	Electron charge, 1.6×10^{-19} C
F	Force, N
$\mathbf{F}_v$	Electric vector potential
g	Acceleration due to Earth gravity at sea level, m/s^2
h	Resonant cavity height, m
h_e	Exit enthalpy, J
h_0	Stagnation enthalpy, J
I_{sp}	Specific impulse, s
j	$\sqrt{-1}$
J_m	Bessel function of the first kind
K	Boltzmann's constant, 1.38×10^{-23} J/K
L	Characteristic dimension, m
N_D	Number of particles in Debye sheath
n	Charge concentration, m^{-3}
M	Mach number
$\bar{M}$	Propellant molecular weight, kg/mol
M_e	Exit Mach number
m	Mass, kg
$\dot{m}$	Mass flow rate, kg/s
P_{for}	Forward power, W
P_{inp}	Input power, W
P_{ref}	Reflected power, W
p	Pressure, Pa
p_a	Ambient pressure, Pa
p_e	Nozzle exit pressure, Pa
p_0	Stagnation pressure, Pa
R	Gas constant, J/mol·K
$\bar{R}$	Universal gas constant, 8.314 J/mol·K
T	Temperature, K
T_e	Electron temperature, K
T_0	Stagnation temperature, K
t	Dielectric thickness, m
u_e	Nozzle exit velocity, m/s
u_{eq}	Equivalent nozzle exit velocity, m/s
V_t	Breakdown voltage, V
Y_m	Bessel function of the second kind

β Phase constant

γ Ratio of specific heats

$\bar{\gamma}$ Secondary emission coefficient

ε Permittivity, F/m

ε_0 Permittivity of free space, 8.854×10^{-12} F/m

Λ Diffusion length, m

λ_D Debye length, m

μ Permeability, H/m

$\bar{\rho}$ Density, kg/m^3

$\bar{\rho}_0$ Stagnation density, kg/m^3

τ_c Mean time between collisions, s

τ Thrust, N

χ_{mn} nth zero of the order m of the Bessel function J_m

ω_p Frequency of plasma oscillations, Hz

ω Field radian frequency, Hz

ACKNOWLEDGMENTS

This project was, first and foremost, a great hands-on experience and I would like to thank the people that helped me along. I'd like to thank my adviser, Dr. Sven Bilén, for his continued patience and support. I would also like to thank Dr. Michael Micci for his contributions and expertise. Richard Auhl helped with a lot of fabrication and was very understanding of an often unpredictable schedule. Philip Mainwaring was present for the final stages of the project and was very helpful during some of the most stressful times. Finally, Jesse McTernan was a constant source of help and advice, for which I am extremely thankful.

Chapter 1

Introduction

Picosatellites provide a very useful platform for small-scale in-space experiments, educational projects, and missions with low power and size requirements. The CubeSat standard, which is becoming increasingly more popular, is well suited to certain types of missions, such as atmospheric, radio, and imaging experiments. However, these and other missions are limited in possible scope by their lack of propulsion options. Their small size means it is currently not feasible to include a system that would allow orbit transfer. A CubeSat-scale microwave electrothermal thruster (MET) would broaden the mission scope of CubeSats by providing a propulsion system compact and simple enough to be put onboard this or other types of small satellites.

1.1 Motivation

Access to space has generally been available to only a few institutions due to prohibitive costs and complexity. Recent developments in technology have made it feasible to perform effective missions using miniature satellites. CubeSats in particular are a popular platform for university-lead teams. These miniature satellites are cost-effective, and the standardized platform reduces complexity.

Satellites often have to adjust attitude or perform orbital maneuvers as part of their missions. Small satellites like CubeSats, however, are not able to perform any significant maneuvers due to their very limited propulsion options. The vast majority of past CubeSat missions have not included a propulsion system. The standard has very stringent volume and mass requirements that make launching a satellite easier, but at the same time make it hard to incorporate a substantial propulsion system. This lack of propulsion limits the types of missions that CubeSats can undertake. In addition, some opponents of the CubeSat standard point out that, due to an inability to deorbit at the end of their lifetimes, CubeSats might become "space junk", which makes the space environment more dangerous for other functioning satellites. An effective propulsion system would alleviate those concerns and open up a whole new scope of possible missions to picosatellites. The use of "green" propellants on CubeSats is desirable as well. A common propellant in use today is hydrazine, which is toxic and corrosive. Minimizing the use of specialized equipment for handling of propellant would further reduce costs of small satellite propulsion systems.

METs can use a wide range of "green" propellants and can be made small enough to be used onboard CubeSats or similar small satellites. A CubeSat-scale MET module can fulfil the need for propulsion, further expanding mission capabilities of very small satellites and making a wider range of missions affordable to university and small-budget groups.

1.2 Contributions

Previous work established some theoretical expectations for an MET operating in the K_u-band, as well as determined the dimensions of the resonant cavity. This thesis aimed to gather the first set of experimental data for a CubeSat-scale microwave electrothermal thruster in this frequency range. To accomplish this, a thruster head laboratory prototype was designed and machined. The height of its candlestick antenna was optimized. All the necessary microwave power and propellant system components were assembled for laboratory plasma ignition tests. Plasma ignition was performed with helium propellant, and the system was later modified to allow ignition testing with ammonia propellant. These tests will serve as the foundation for further optimization of the K_u-band thruster design.

1.3 Thesis Overview

This thesis describes the design, manufacture, and initial testing of a microwave electrothermal thruster at 17.8 GHz. Chapter 2 details background on propulsion systems, in general, and the theoretical background relevant to MET operation. Chapter 3 discusses the design process of the prototype thruster head, as well as some guidelines for expanding the project to other subsystems of a full CubeSat-scale propulsion module. Chapter 4 presents the experimental setup assembled to test plasma ignition in the thruster head using helium propellant, as well as experimental results of those tests. Initial experimental setup for ammonia propellant testing is also discussed. Finally, Chapter 5 provides conclusions drawn from this work and suggestions for future research.

Chapter 2

Background

2.1 Thruster Background

2.1.1 Rocket Propulsion Overview

Space propulsion refers to any device that provides kinetic energy to a spacecraft for movement. The majority of these devices operate by accelerating a propellant out of a control volume and are usually categorized as either chemical or electric propulsion. Chemical rockets are characterized by accelerating propellant via chemical reactions, such as heat of combustion. The propellant can be stored as either a liquid or solid. Chemical rockets are the most common space propulsion devices in use today. Both solid and liquid propellant rockets are well-understood and usually serve in applications that require high thrust. Rockets lifting off from the Earth, for example, require very high thrust to overcome gravity.

Electric rockets accelerate propellant through electrical means. Electric devices can be further categorized into electrostatic, electromagnetic, or electrothermal methods. Electrostatic devices use electric fields to accelerate propellant and include Hall thrusters and ion thrusters. Electromagnetic devices use electromagnetic fields to accelerate propellant, and include pulsed plasma thrusters. Electrothermal propulsion uses electricity to heat up a propellant to accelerate it; arcjet and resistojet thrusters are examples. Microwave electrothermal thrusters also fall under this category. Electric rockets usually provide a low thrust, but a very high efficiency and can be operated for long periods of time. They are not suitable for liftoff, but can be perfect for satellite station keeping and maneuvering on long-term missions.

2.1.2 Rocket Performance Characterization

Rockets are governed by Newton's laws of motion. Those principles can be used to derive thrust, which is one of the benchmarks by which rocket performance is measured. Thrust is a reaction force that acts in the direction opposite of rocket exhaust velocity. A rocket can be visualized as a control volume, as shown in Figure 2.1.

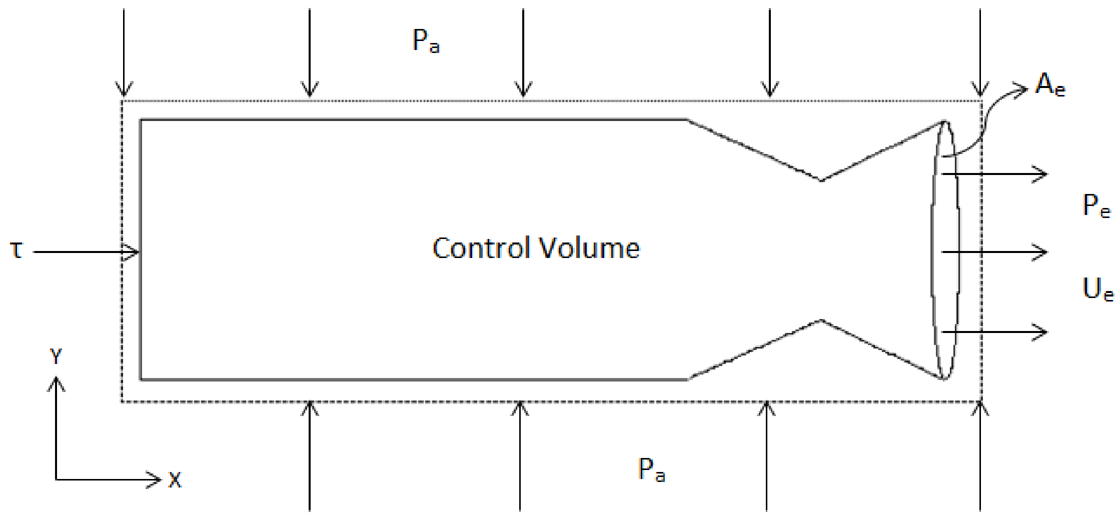

Figure 2.1: Control volume for generalized rocket system

Forces in the vertical, or y-direction, are equal and opposite, so they can be ignored. The sum of forces in the x-direction can be written as[1]

$$\sum F_x = \tau + A_e p_a - A_e p_e. \tag{2.1}$$

The control volume from Figure 2.1 does not allow momentum flux from outside to inside, so the forces can only be related to momentum flux from inside to outside. This can be written as[1]

$$\sum F_x = \int \rho u_x (\mathbf{u} \bullet \mathbf{n}) dA = \dot{m} u_e. \tag{2.2}$$

Combining Equations (2.1) and (2.2), it can be shown that thrust is[1]

$$\tau = \dot{m} u_e + A_e (p_e - p_a), \tag{2.3}$$

which shows that thrust depends on the amount of mass accelerated out of the control volume, as well as the exhaust velocity. This helps explain the differences in thrust between chemical and electric rockets. A chemical rocket can have enormous mass flow rate and very high internal pressures. By comparison, electric rockets tend to have very high exhaust velocities, but much smaller flow rates and internal pressures.

Thrust can also be expressed in terms of equivalent velocity. Equivalent velocity incorporates exhaust velocity and pressure change, i.e.,[1]

$$u_{\mathrm{eq}} = u_e + \frac{A_e(p_e - p_a)}{\dot{m}}. \tag{2.4}$$

This allows thrust to be expressed as momentum only, i.e.,[1]

$$\tau = \dot{m} u_{\mathrm{eq}}. \tag{2.5}$$

Another important performance metric for rockets is specific impulse. This quantity corresponds to the propellant efficiency of the rocket or thruster. Specific impulse can be expressed as[1]

$$I_{\mathrm{sp}} = \frac{\tau}{\dot{m} g} = \frac{u_{\mathrm{eq}}}{g}. \tag{2.6}$$

Electric propulsion devices tend to have high equivalent velocities due to high nozzle exit velocities, and, correspondingly, have high specific impulses. High specific impulse makes electric propulsion a good choice for mass-restricted missions.

2.1.3 Isentropic Relations in Rocket Thrust Chambers

Rockets that utilize a pressure chamber, such as chemical rockets or electrothermal rockets like the MET, can be analytically examined by first making three important assumptions. First, the working fluid is an ideal gas of constant composition. The equation of state for an ideal gas is[1]

$$p = \bar{\rho}RT. \tag{2.7}$$

Second, the heating process in the chamber is assumed to be constant-pressure. Finally, the process must be steady, one-dimensional, and isentropic.[1]

Conditions inside the pressure chamber can be described as being in a stagnation state. Stagnation state is reached when a fluid is brought to rest reversibly, adiabatically, and without work.[1] Considering the flow assumptions, stagnation state pressure and temperature can be related through[1]

$$\frac{p_0}{p} = \left(\frac{T_0}{T}\right)^{\frac{\gamma}{(\gamma-1)}}. \tag{2.8}$$

This is a useful relation because chamber pressure and temperature are usually easier to measure than properties in other parts of the rocket system. The pressure ratio can also be related to the Mach number, M, which is defined as[1]

$$M = \frac{u}{a}, \tag{2.9}$$

where[1]

$$a = \sqrt{\gamma RT}. \tag{2.10}$$

The pressure-ratio-to-Mach-number relation can be expressed as[1]

$$\frac{p_0}{p} = \left(1 + \frac{\gamma - 1}{2}M^2\right)^{\gamma/(\gamma-1)}. \tag{2.11}$$

When applied to the nozzle exit pressure, Equation (2.11) becomes[1]

$$\frac{p_0}{p_e} = \left(1 + \frac{\gamma - 1}{2}M_e^2\right)^{\gamma/(\gamma-1)}. \tag{2.12}$$

In the case of a nozzle without a diverging portion, the Mach number can be assumed to be $M_e = 1$. This assumptions simplifies Equation (2.12) to[1]

$$\frac{p_e}{p_0} = \left(\frac{2}{\gamma + 1}\right)^{\gamma/(\gamma-1)}. \tag{2.13}$$

The temperature ratio can also be rewritten in terms of the Mach number as[1]

$$\frac{T_0}{T} = 1 + \frac{\gamma - 1}{2} M^2. \tag{2.14}$$

The same can also be done to the density ratio by using Equations (2.7), (2.11), and (2.14):[1]

$$\frac{\bar{\rho}_0}{\bar{\rho}} = \left(1 + \frac{\gamma - 1}{2} M^2\right)^{\frac{1}{(\gamma-1)}}. \tag{2.15}$$

Equations (2.9), (2.10), and (2.14) can then be used to define the velocity of the flow as[1]

$$u = M \sqrt{\frac{\gamma R T_0}{1 + \frac{\gamma - 1}{2} M^2}}. \tag{2.16}$$

With this form of the velocity and Equation (2.15), mass flow rate inside a rocket can be written in terms of isentropic relations as[1]

$$\frac{\dot{m}}{A} = \frac{p_0 \sqrt{\gamma}}{\sqrt{R T_0}} M \left(\frac{1}{1 + \frac{\gamma - 1}{2} M^2}\right)^{\frac{\gamma+1}{2(\gamma-1)}}. \tag{2.17}$$

In a rocket system, the mass flow rate per area is maximum when the Mach number $M = 1$. This state of maximum flow reduces Equation (2.17) to[1]

$$\frac{\dot{m}}{A^*} = \frac{p_0}{\sqrt{R T_0}} \sqrt{\gamma} \left(\frac{2}{\gamma + 1}\right)^{\frac{\gamma+1}{2(\gamma-1)}}. \tag{2.18}$$

Creating a ratio of Equations (2.17) and (2.18) allows us to create a relation between the A^* condition and the area of the flow:[1]

$$\boldsymbol{\frac{A}{A^*} = \frac{1}{M} \left[\frac{2}{\gamma + 1}\left(1 + \frac{\gamma - 1}{2} M^2\right)\right]^{\frac{\gamma+1}{2(\gamma-1)}}}. \tag{2.19}$$

Similarly to the pressure ratio from Equation (2.12), the area ratio in Equation (2.19) can be applied to specifically investigate exit are with[1]

$$\boldsymbol{\frac{A_e}{A^*} = \frac{1}{M_e}\left[\frac{2}{\gamma+1}\left(1+\frac{\gamma-1}{2}M_e^2\right)\right]^{\frac{\gamma+1}{2(\gamma-1)}}}. \tag{2.20}$$

For further analysis, assuming adiabatic nozzle expansion, conservation of energy can be used to define the relationship between stagnation enthalpy and nozzle exit enthalpy, i.e.,[1]

$$\frac{u_e^2}{2} = h_0 - h_e = c_p(T_0 - T_e). \tag{2.21}$$

If the expansion is also isentropic, Equation (2.8) can be substituted into Equation (2.21) to obtain an expression for u_e:[1]

$$u_e = \sqrt{\frac{2\gamma\bar{R}}{(\gamma-1)\bar{M}}T_0\left[1-\left(\frac{p_e}{p_0}\right)^{\frac{\gamma-1}{\gamma}}\right]}. \tag{2.22}$$

Substituting Equation (2.18) for the mass flow and Equation (2.22) for the exit velocity in Equation (2.3), the thrust can additionally be found by[1]

$$\frac{\tau}{A^* p_0} = \sqrt{\frac{2\gamma^2}{\gamma-1}\left(\frac{2}{\gamma+1}\right)^{\frac{\gamma+1}{\gamma-1}}\left[1-\left(\frac{p_e}{p_0}\right)^{\frac{\gamma-1}{\gamma}}\right]} + \left(\frac{p_e}{p_0}-\frac{p_a}{p_0}\right)\frac{A_e}{A^*}. \tag{2.23}$$

2.1.4 MET Overview

Microwave electrothermal thrusters are a type of electric propulsion that use the thermal energy from a plasma to heat and accelerate propellant. Figure 2.2 shows a cross-section view schematic of an MET.

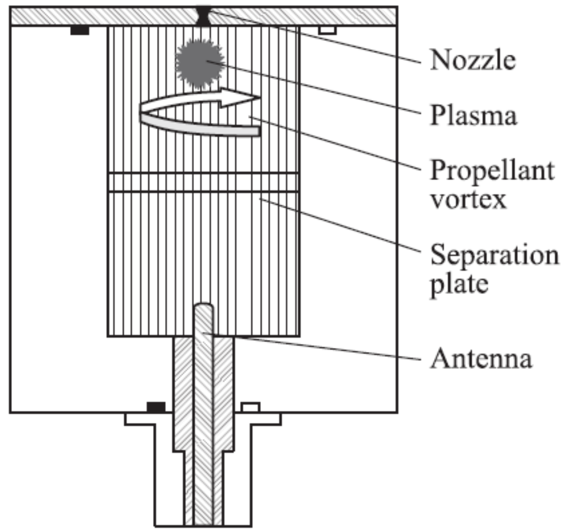

Figure 2.2: Thruster cavity cross section[2]

The thruster body primarily consists of a circular resonant cavity sized appropriately for the desired frequency range for operation. The microwave antenna placed at the bottom of the cavity transmits microwave energy into the cavity, creating a TM^z_{011} resonant mode. Figure 2.3 shows the resultant electric and magnetic fields.

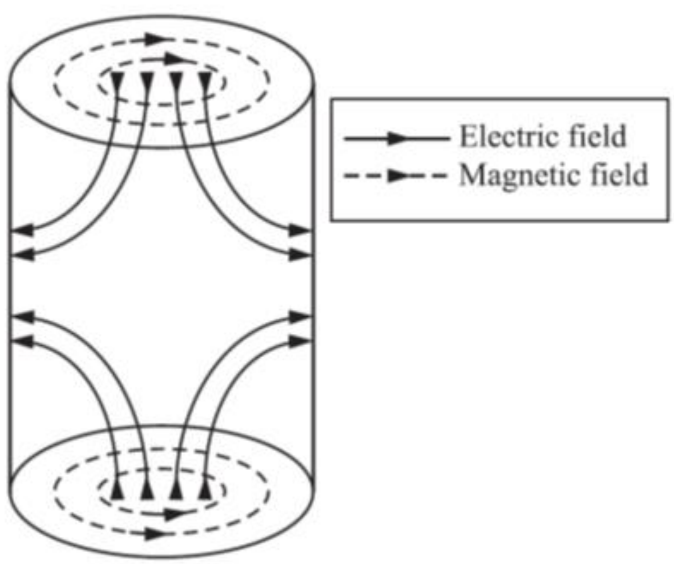

Figure 2.3: TM^z_{011} resonant mode in a circular cavity[2]

As Figure 2.3 shows, the resonant mode concentrates electric field lines near the flat ends of the cavity, and lower concentrations at the midplane of the cavity. This configuration places the highest electric field concentrations near the antenna and the nozzle. Propellant ports are placed tangentially to the cavity wall and near the nozzle in order to inject propellant close to the area of high energy density and to create a propellant vortex. In order for plasma to form, the cavity needs to be at a pressure that corresponds to the desired power for breakdown.[3] With high electric field density, propellant flowing, and appropriate pressure, a plasma ignites within the cavity. The propellant vortex helps cool the cavity walls and keeps the plasma away by stabilizing it in the center of the cavity. After ignition, the internal pressure of the thruster rises while maintaining the plasma itself. This stable plasma heats all incoming propellant, accelerating it out of the nozzle to produce thrust.

As Figure 2.3 demonstrates, electric field density is high near the antenna, not just the nozzle, in TM^{z}_{011} resonant mode. Because of this, most MET models separate the two regions using a dielectric plate placed at the midplane, as seen in Figure 2.2, where it symmetrically perturbs the electric energy density. Other versions of the thruster feature a dielectric cap placed over the antenna at the bottom of the cavity.[3] The dielectric protects the antenna by either physically insulating it with a cap, or keeping the cavity half near the antenna at a higher pressure to inhibit plasma ignition.

2.1.5 Previous Work on METs

Research on METs has been progressing at Penn State since the 1980s, beginning with Micci, Maul, and Balaam.[4] The first prototype thruster cavity was fabricated by Sullivan and Micci.[5] The thruster operated at a frequency of 2.45 GHz and had a cavity radius of 8.89 cm. It also included a movable short that allowed its length to be adjusted. This feature allowed the cavity to operate in both TM^{z}_{011} and TM^{z}_{012} modes. Experiments using the TM^{z}_{011} mode reached powers upwards of 2000 W. These experiments investigated plasma formation and stability inside a resonant cavity, effects of different propellants on plasma formation, and effects of dielectric inserts. Kline[6] further refined the thruster and performed the first set of thrust measurements. His MET produced a maximum thrust of 303 mN using 800 W of incident power.

Nordling[7] continued research into electrothermal plasma propulsion using a 7.5-GHz MET developed with assistance from Research Support Instruments of Landham, Maryland. This cavity had a radius of 2.58 cm and a height of 3.32 cm. This smaller cavity was intended to be used on a small spacecraft with lower power and lower thrust requirements. Nordling's main goal was to perform thrust stand testing with helium and nitrogen propellants. Helium yielded a maximum thrust of 7.66 mN at 159 W and nitrogen yielded 13.77 mN at 200 W.

Souliez[8] continued research into low-power operation, examining both the 2.45-GHz and 7.5-GHz cavities. At powers of less than 100 W, the 2.45-GHz cavity was not able to maintain plasma ignition at chamber pressures that would be useful for space propulsion. The 7.5-GHz thruster, on the other hand, was able to maintain ignition in vacuum. Thrust stand results showed 22 mN of thrust using helium propellant and 20 mN of thrust using nitrogen propellant.

Roos[9] expanded on this work by performing another set of thrust stand measurements in atmospheric conditions and obtaining similar results to Souliez. The thrust stand was tested in vacuum environment with helium propellant for the first time as well. Only cold-flow thrust measurements without input power were made, reaching 15.14 mN.

Work by Welander[10] attempted to continue vacuum thrust measurements, but ran into problems with equipment that resulted in unsatisfying data. The thrust measurement apparatus used a momentum trap and strain gage flexure, and it was suspected that incorrect measurements resulted from issues with this setup.

Further efforts by Clemens[11] attempted to modify the momentum trap and strain gage apparatus to produce accurate vacuum thrust measurements. The new design allowed the thruster exhaust stream to escape the momentum trap more effectively, preventing a pressure buildup that was causing inaccurate measurements in the previous design. Cold-gas testing yielded results that agreed within 90–100% of theoretical calculations. Hot-gas testing, however, did not show any successful results. It was discovered that the thruster exhaust transferred too much heat to the strain gage flexure, causing inaccurate measurements. Clemens[12] continued his research on METs, focusing his efforts on testing the 7.5-GHz and 2.45-GHz cavities with ammonia and simulated hydrazine propellants. Thrust and specific impulse measurements were made and it was discovered that, since tested MET models were not optimized for hydrazine propellant, measured performance figures were up to 40% lower than theoretical predictions. Numerical modeling helped design a new 8-GHz thruster, which performed better than the previous model in preliminary testing.

Blum[13] continued work on the 8-GHz MET with an attempt to experimentally determine the optimum thruster configuration. In his experiments, Blum varied the antenna depth, propellant injector cross-sectional diameter, nozzle material and throat diameter, and propellant type. His resulting optimum thruster used ammonia propellant and achieved thermal efficiencies of 75% with a specific impulse 33% higher than any previous MET running ammonia.

Most recently, Hopkins[14] followed up on improvements to the 8-GHz MET made by Blum. This involved changing cavity material from aluminum to steel for better electrical properties, updating the diverging–converging nozzle, and using boron nitride for the separation plate. Improvements to the vacuum thrust stand apparatus were also made, which yielded more accurate and repeatable results than possible with older equipment. Some work remains, as even this improved apparatus returns relatively large measurement errors.

While others were concerned with perfecting the 8-GHz thruster, Goovaerts[15] began work on a smaller MET. The goal was to create a more economical thruster that could operate on spacecraft with small power and size budgets. The result was a feasibility study for a 14.5-GHz MET with a cavity height of 2.1 cm and a diameter of 1.3 cm. The prototype went through cold-flow and hot-flow tests. Maximum input power was set at 20 W. This early attempt achieved plasma ignition; however, there were repeatability issues and low efficiency, possibly due to low electric field strength.

Adusumilli[16] built upon the low-power 14.5-GHz MET, and performed a number of experiments using a modified, higher power thruster. This cavity had a number of modifications that allowed it to run at 100 W. Hot-fire testing achieved 96% coupling efficiency and theoretical thrust of 11 mN with a specific impulse of 422 s.

Capalungan[17] was involved in the latest developments in MET research. The ultimate goal of MET scaling projects is to create a feasible propulsion system for a small spacecraft. Capalungan's 30-GHz MET was the smallest model yet, having a height of only 1.43 cm and a radius of 0.87 cm. A prototype was constructed but never tested due to limitations of microwave equipment. Because the MET was so small and operated at such a high frequency, its tolerances were extremely tight. In addition, the space-rated microwave equipment that can operate at such a high frequency is generally very expensive and with lower efficiency. While the small size was ideal, these issues prevented 30 GHz from being the optimal frequency for MET operation, and future projects need to find an acceptable balance between size and availability of microwave equipment.

2.2 Cavity Theory

2.2.1 Electromagnetic Resonance in Circular Cavities

Plasma inside the MET cavity forms due to microwave breakdown of the injected gas in a region of high electric fields. The electric field equations can be derived from the magnetic vector potential and from the electric and magnetic wave equations. An MET cavity is formed by shorting the ends of a circular waveguide, so a cylindrical coordinate system, like the one shown in Figure 2.4, is convenient for theoretical analysis.

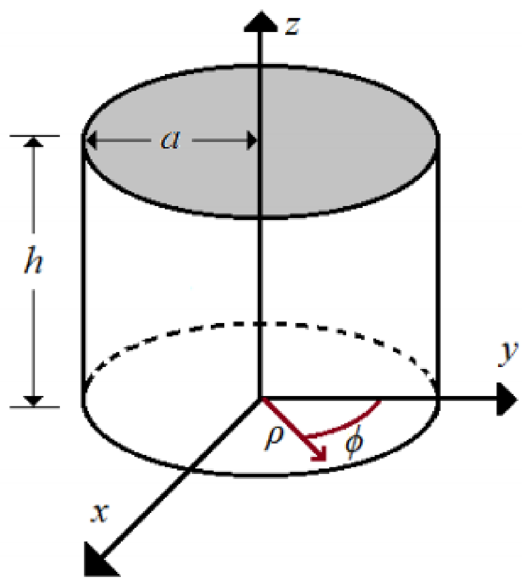

Figure 2.4: Resonant cavity cylindrical coordinate system[16]

Analysis of the MET resonant cavity begins by defining magnetic vector potential **A** and electric vector potential $\mathbf{F}_v$. For transverse magnetic to z (TM^z) modes, the vector potentials are[18]

$$\mathbf{A} = \hat{\boldsymbol{a}}_z A_z(\rho, \phi, z), \qquad \textbf{(2.24)}$$

$$\mathbf{F}_v = 0. \qquad \textbf{(2.25)}$$

The vector potential **A** must satisfy the vector wave equation, i.e.,[39]

$$\nabla^2 A_z(\rho, \phi, z) + \beta^2 A_z(\rho, \phi, z) = 0. \qquad \textbf{(2.26)}$$

The solution to Equation (2.26) can be written as[18]

$$A_z(\rho,\phi,z) = [A_1 J_m(\beta_\rho \rho) + B_1 Y_m(\beta_\rho \rho)] \times$$
$$[C_2 \cos(m\phi) + D_2 \sin(m\phi)][A_3 e^{-j\beta_z z} + B_3 e^{j\beta_z z}], \qquad m = 0, 1, 2 \ldots \tag{2.27}$$

The β_ρ and β_z constants are components of the phase constant, and are related through the constraint equation, i.e.,[18]

$$\beta_\rho^2 + \beta_z^2 = \beta^2. \tag{2.28}$$

In order to solve for the constants A_1, B_1, C_2, D_2, A_3, and B_3, in Equation (2.27), boundary conditions must be applied. The constant B_1 must be zero due to the fact that the fields must be finite everywhere ($Y_m(\rho = 0) = \infty$). It can also be assumed that the fields must repeat every 2π radians. In addition, the following boundary conditions can be applied[18]

$$E_\phi(\rho = a, \phi, z) = 0, \tag{2.29}$$

$$E_z(\rho = a, \phi, z) = 0. \tag{2.30}$$

Because the transverse magnetic modes to z are being considered, it can be assumed that waves propagate only in the $+z$ direction. Due to this, and the boundary conditions, Equation (2.27) can be simplified to[18]

$$A_z^+(\rho,\phi,z) = B_{mn} J_m(\beta_\rho \rho)[C_2 \cos(m\phi) + D_2 \sin(m\phi)] e^{-j\beta_z z}, \tag{2.31}$$

which can also be expressed as[18]

$$A_z^+(\rho,\phi,z) = B_{mn} J_m(\beta_\rho \rho)[C_2 \cos(m\phi) + D_2 \sin(m\phi)] \times [C_3 \cos(\beta_z z) + D_3 \sin(\beta_z z)]. \tag{2.32}$$

With the magnetic vector potential defined, it can now be used in conjunction with electric and magnetic field components. For a TM^z cylindrical coordinate system, the electric and magnetic field components can be written as[18]

$$E_\rho = -j\frac{1}{\omega\mu\varepsilon}\frac{\partial^2 A_z}{\partial\rho\partial z}, \tag{2.33}$$

$$E_\phi = -j\frac{1}{\omega\mu\varepsilon}\frac{1}{\rho}\frac{\partial^2 A_z}{\partial\phi\partial z}, \tag{2.34}$$

$$E_z = -j\frac{1}{\omega\mu\varepsilon}\left(\frac{\partial^2}{\partial z^2} + \beta^2\right)A_z, \tag{2.35}$$

$$H_\rho = \frac{1}{\mu}\frac{1}{\rho}\frac{\partial A_z}{\partial\phi}, \tag{2.36}$$

$$H_\phi = -\frac{1}{\mu}\frac{\partial A_z}{\partial\rho}, \tag{2.37}$$

$$H_z = 0. \tag{2.38}$$

Equation (2.32) can now be used to rewrite the E_ϕ component from Equation (2.34) as[18]

$$\begin{aligned} E_\phi(\rho,\phi,z) = -jB_{mn}\frac{m\beta_z}{\omega\mu\varepsilon}\frac{1}{\rho}J_m(\beta_\rho\rho)[-C_2\sin(m\phi) + D_2\cos(m\phi)] \\ \times[-C_3\sin(\beta_z z) + D_3\cos(\beta_z z)]. \end{aligned} \tag{2.39}$$

Similarly, Equation (2.31) can be used to rewrite the E_z component from Equation (2.35) as[18]

$$E_z = -jB_m\frac{\beta_\rho^2}{\omega\mu\varepsilon}J_m(\beta_\rho\rho)[C_2\cos(m\phi) + D_2\sin(m\phi)]e^{-j\beta_z z}. \tag{2.40}$$

Equations (2.39) and (2.40) can now be used to solve for the phase constant components β_z and β_ρ, respectively. Applying the boundary condition in Equation (2.30) to Equation (2.40) yields[18]

$$E_z(\rho = a,\phi,z) = -jB_{mn}\frac{\beta_\rho^2}{\omega\mu\varepsilon}J_m(\beta_\rho a)[C_2\cos(m\phi) + D_2\sin(m\phi)]e^{-j\beta_z z} = 0. \tag{2.41}$$

This relationship only holds true if[18]

$$J_m(\beta_\rho a) = 0 \Rightarrow \beta_\rho a = \chi_{mn} \Rightarrow \beta_\rho = \frac{\chi_{mn}}{a}, \tag{2.42}$$

where χ_{mn} is the nth zero of the Bessel function J_m and of the order m. These zeroes can be found tabulated in the literature, such as in Balanis.[18] In order to solve for the phase component β_z, additional boundary conditions must be applied, i.e.,[18]

$$E_\phi(0 \le \rho \le a, 0 \le \phi \le 2\pi, z = 0) = E_\phi(0 \le \rho \le a, 0 \le \phi \le 2\pi, z = h) = 0. \quad \textbf{(2.43)}$$

The boundary conditions in Equation (2.43) are the result of cavity's end plates. When Equation (2.43) is applied to Equation (2.39), the E_ϕ component can then be used to solve for β_z:[18]

$$\begin{aligned} &E_\phi(0 \le \rho \le a, 0 \le \phi \le 2\pi, z = 0) \\ &\qquad = -jB_{mn}\frac{m\beta_z}{\omega\mu\varepsilon}\frac{1}{\rho}J_m(\beta_\rho\rho)[-C_2\sin(m\phi) + D_2\cos(m\phi)] \\ &\qquad \times [-C_3(0) + D_3(1)] = 0 \Rightarrow D_3 = 0, \end{aligned} \quad \textbf{(2.44)}$$

$$\begin{aligned} &E_\phi(0 \le \rho \le a, 0 \le \phi \le 2\pi, z = h) \\ &\qquad = jB_m\frac{m\beta_z}{\omega\mu\varepsilon}\frac{1}{\rho}J_m\left(\beta_\rho\rho\right)[-C_2\sin(m\phi) + D_2\cos(m\phi)] \\ &\qquad \times [C_3\sin(\beta_z h)] = 0, \\ &\sin(\beta_z h) = 0 \Rightarrow \beta_z h = \sin^{-1}(0) = p\pi \Rightarrow \beta_z = \frac{p\pi}{h}\ ; \ \ p = 0,1,2,3, \dots \end{aligned} \quad \textbf{(2.45)}$$

Using both components of the phase constant from Equations (2.42) and (2.45), the resonant frequency can be obtained by using the relationship from Equation (2.28):[18]

$$\beta_\rho^2 + \beta_z^2 = \left(\frac{\chi_{mn}}{a}\right)^2 + \left(\frac{p\pi}{h}\right)^2 = \beta_r^2 = \omega_r^2\mu\varepsilon, \quad \textbf{(2.46)}$$

hence,[39]

$$(f_r)_{mnp}^{\mathrm{TM}^z} = \frac{1}{2\pi\sqrt{\mu\varepsilon}}\sqrt{\left(\frac{\chi_{mn}}{a}\right)^2 + \left(\frac{p\pi}{h}\right)^2}, \quad \textbf{(2.47)}$$

where[39]

$$m = 0, 1, 2,3, \dots\ ; n = 1, 2, 3, \dots\ ; p = 0, 1, 2, 3, \dots \quad \textbf{(2.48)}$$

In the case of an MET circular resonant cavity, the mode of interest is $\mathrm{TM}^z{}_{011}$, meaning that the appropriate resonant frequency equation is

$$(f_r)_{011}^{\mathrm{TM}^z} = \frac{1}{2\pi\sqrt{\mu\varepsilon}}\sqrt{\left(\frac{\chi_{01}}{a}\right)^2 + \left(\frac{\pi}{h}\right)^2}. \quad \textbf{(2.49)}$$

2.2.2 Resonance in Partially Filled Cavities

Designs of many previous MET models included a dielectric insert in the cavity in order to protect the antenna from hot plasma. The 17.8-GHz MET also includes a thin dielectric plate positioned at the midplane of the cavity.

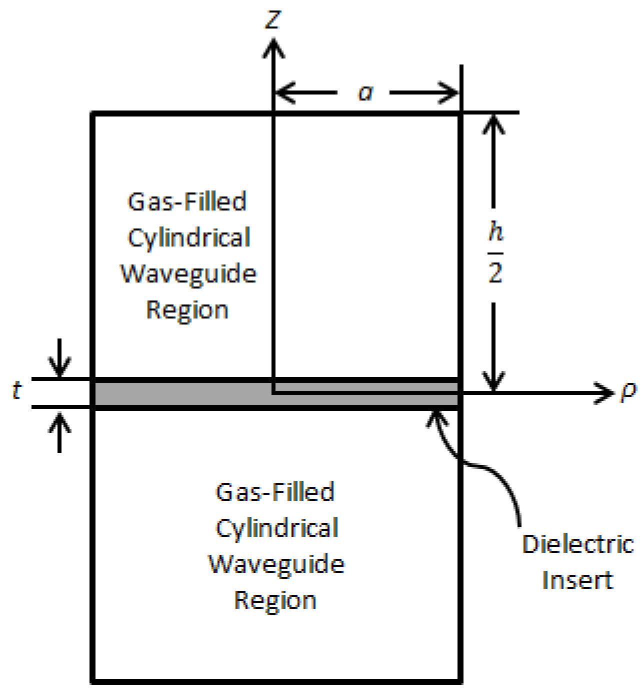

Figure 2.5: Generalized dimensions of a resonant cavity with dielectric insert

A process similar to the one described in Section 2.2.1 can be used to find resonant frequencies of a cavity with this configuration. A coordinate system like the one described in Figure 2.4 can once again be assumed. Dimensions for the cavity and dielectric insert are defined as shown in Figure 2.5. The vector potential for the upper section of a partially filled cavity can be split into two regions. The gas-filled region vector potential is described as[19]

$$A_{z,g} = B_{mnp,g} J_m(\beta_\rho \rho) \cos(m\phi) \cos\left[\beta_{z,g}\left(\frac{h}{2} - z\right)\right], \tag{2.50}$$

$$\beta_\rho^2 + \beta_{z,g}^2 = \beta_{\mathrm{res},g}^2 = \omega_{\mathrm{res}}^2 \mu_g \varepsilon_g. \tag{2.51}$$

Similarly, the vector potential of the dielectric-filled region of the cavity becomes[19]

$$A_{z,d} = B_{mnp,d} J_m\left(\beta_\rho \rho\right) \cos(m\phi) \cos(\beta_{z,d} z), \tag{2.52}$$

$$\beta_\rho^2 + \beta_{z,d}^2 = \beta_{\mathrm{res},d}^2 = \omega_{\mathrm{res}}^2 \mu_d \varepsilon_d. \tag{2.53}$$

The vector potentials in Equations (2.50) and (2.52) can be combined with Equation (2.33) to rewrite the radial component of the electric field as[19]

$$E_{\rho,g} = -j \frac{B_{mnp,g} \beta_{z,g} \beta_\rho}{\omega \mu_g \varepsilon_g} J_m'(\beta_\rho \rho) \cos(m\phi) \sin\left[\beta_{z,g}\left(\frac{h}{2} - z\right)\right], \tag{2.54}$$

$$E_{\rho,d} = j \frac{B_{mnp,d} \beta_{z,d} \beta_\rho}{\omega \mu_d \varepsilon_d} J_m'(\beta_\rho \rho) \cos(m\phi) \sin(\beta_{z,d} z). \tag{2.55}$$

The boundary conditions described in Equation (2.43) also apply in this case. However, the interaction of the dielectric region with the gas region requires additional boundary conditions. These additional conditions are[19]

$$E_{\rho,d}\left(z = \frac{t}{2}\right) = E_{\rho,g}\left(z = \frac{t}{2}\right), \tag{2.56}$$

$$E_{\phi,d}\left(z = \frac{t}{2}\right) = E_{\phi,g}\left(z = \frac{t}{2}\right), \tag{2.57}$$

$$H_{\rho,d}\left(z = \frac{t}{2}\right) = H_{\rho,g}\left(z = \frac{t}{2}\right), \tag{2.58}$$

$$H_{\phi,d}\left(z = \frac{t}{2}\right) = H_{\phi,g}\left(z = \frac{t}{2}\right). \tag{2.59}$$

The conditions arise from the fact that fields tangential to the interface between the gas and dielectric regions must be continuous. Applying Equation (2.56) to the vector potentials in Equations (2.54) and (2.55) yields a relationship between electric fields in the gas and dielectric regions:[19]

$$\frac{\beta_{mnp,d} \beta_{z,d}}{\mu_d \varepsilon_d} \sin\left(\beta_{z,d} \frac{t}{2}\right) = -\frac{\beta_{mnp,g} \beta_{z,g}}{\mu_g \varepsilon_g} \sin\left[\beta_{z,g}\left(\frac{h}{2} - \frac{t}{2}\right)\right], \tag{2.60}$$

A similar relationship can be defined for the azimuthal components of the magnetic field. Equation (2.37) can be combined with Equations (2.50) and (2.52) to yield the magnetic field component in the gas and dielectric regions, respectively:[19]

$$H_{\phi,g} = -\frac{B_{mnp,g}\beta_\rho}{\mu_g} J_m'(\beta_\rho \rho)\cos(m\phi)\sin\left[\beta_{z,g}\left(\frac{h}{2} - z\right)\right], \quad \textbf{(2.61)}$$

$$H_{\phi,d} = -\frac{B_{mnp,d}\beta_\rho}{\mu_d} J_m'(\beta_\rho \rho)\cos(m\phi)\sin(\beta_{z,d} z)\,. \quad \textbf{(2.62)}$$

As before, the boundary condition in Equation (2.59) can be applied to the field components in Equations (2.61) and (2.62), and the result can be equated to yield a relationship between the magnetic field in the gas and dielectric regions, i.e.,[19]

$$\frac{\beta_{mnp,d}}{\mu_d}\cos\left(\beta_{z,d}\frac{t}{2}\right) = \frac{\beta_{mnp,g}}{\mu_g}\sin\left[\beta_{z,g}\left(\frac{h}{2} - \frac{t}{2}\right)\right]. \quad \textbf{(2.63)}$$

Equation (2.60) can be divided by Equation (2.63), and rearranging of the terms produces the relationship between the z-direction wavenumbers of the gas and dielectric regions:[19]

$$\frac{\beta_{z,d}}{\varepsilon_d}\tan\left(\beta_{z,d}\frac{t}{2}\right) = -\frac{\beta_{z,g}}{\varepsilon_g}\tan\left[\beta_{z,g}\left(\frac{h}{2} - \frac{t}{2}\right)\right]. \quad \textbf{(2.64)}$$

From Equation (2.64), the resonance frequency can be found using the relationship from Equations (2.51) and (2.53), rewritten as[15]

$$\beta_{z,g} = \sqrt{\beta_{g,\mathrm{res}}^2 - \beta_\rho^2} = \sqrt{\omega_{\mathrm{res}}^2 \mu_g \varepsilon_g - \left(\frac{\chi_{mn}}{a}\right)^2}\,, \quad \textbf{(2.65)}$$

$$\beta_{z,d} = \sqrt{\beta_{d,\mathrm{res}}^2 - \beta_\rho^2} = \sqrt{\omega_{\mathrm{res}}^2 \mu_d \varepsilon_d - \left(\frac{\chi_{mn}}{a}\right)^2}\,. \quad \textbf{(2.66)}$$

In general, the resonant frequency of a cavity partially filled with dielectric is lower than the resonant frequency of a similarly sized empty cavity. Since the resonant frequency increases as the dimensions of a cavity are made smaller, inserting a dielectric can be used to bring that frequency back down to desirable ranges while achieving compact thruster size.

2.3 Plasma Theory

2.3.1 Plasma Definition and Physics

Many types of electric propulsion, including METs, ionize their propellant gasses, creating charged particles in the form of free electrons and ions. Collections of these charged particles are called plasmas. Plasmas move in response to fields that are generated internally or applied externally. Plasmas are considered electrically "quasineutral" due to equal densities of electrons and positive ions, but electromagnetic forces can still affect them. There are three primary criteria that distinguish between plasma and weakly ionized gas.

Charged particles interact with one another through the Coulomb force. This force causes all the other nearby charged particles around a charge to move. As part of this movement, surrounding charges reduce, or shield, the electric field of any one charge. Once equilibrium is reached, the charged particle accumulates a "cloud". This cloud has a scale length, called the Debye length. The scale length of a plasma as a whole is determined from the Debye lengths of all the species that make up that plasma. For the simple case of an electron, the Debye length can be expressed as[20]

$$\lambda_D = \left(\frac{\epsilon_0 K T_e}{n e^2}\right)^{\frac{1}{2}}. \tag{2.67}$$

In Equation (2.67), particle density is in the denominator, which means that as the density is increased, the Debye length decreases. One of the criteria for distinguishing ionized gas from plasma is that the density must be large enough for the Debye length to be much smaller than the dimension L of the system of interest. This can also be expressed as[20]

$$\lambda_D \ll L. \tag{2.68}$$

In order for a system of charged particles to exhibit plasma collective behavior, it must be made up of enough particles. The number of particles in a sphere with a radius of a Debye length can be found using[20]

$$N_D = n\frac{4}{3}\pi\lambda_D^3. \tag{2.69}$$

This expression also defines the second criterion necessary for a plasma, which can be rewritten as[20]

$$N_D \gg 1. \tag{2.70}$$

Weakly ionized gas and plasma are also separated by the mechanics of internal particle collisions. Ionized particles occasionally impact neutral atoms. In the case of ionized gas, this happens often enough for the gas as a whole to be subject to hydrodynamic forces, same as any gas. A plasma is governed primarily by electromagnetic forces, so there has to be only a small number of collisions between ionized particles and neutral atoms. This third plasma criterion can be expressed by[20]

$$\omega_p\tau_c > 1, \tag{2.71}$$

where ω_p stands for the frequency of plasma oscillations and τ_c represents the mean time between collisions.

2.3.2 Ionization and Gas Breakdown in Microwave Fields

In order for plasma to form in the MET cavity, the propellant must undergo electric breakdown. Electric breakdown, by definition, occurs when a nonconductor becomes a conductor when under the influence of a strong enough electric field.[21] The most significant process that drives electric breakdown is electron avalanche. The process starts with a single electron that is accelerated by an applied field. If enough energy is imparted to the electron, it can ionize another molecule. This ionized molecule produces additional electrons, which are in turn accelerated by the field and can go on to ionize other molecules, creating an avalanche effect and inducing electric breakdown.

However, in order for the avalanche process to begin, certain conditions in the medium must be met. There is generally little noticeable activity in the medium until threshold breakdown conditions are met, and then the electron avalanche process occurs rapidly to complete the breakdown. Plasma in an MET cavity requires there to be a discharge, which is achieved by reaching a breakdown voltage V_t, and the corresponding breakdown field E_t. These quantities can first be examined in a simple case consisting of breakdown between two electrodes, which has some differences from breakdown in a cavity. The breakdown conditions can be expressed as[21]

$$V_t = \frac{B(pd)}{C + \ln pd}, \tag{2.72}$$

$$\frac{E_t}{p} = \frac{B}{C + \ln pd}. \tag{2.73}$$

The constant C in Equations (2.72) and (2.73) is equal to[21]

$$C = \ln\left(\frac{A}{\ln\left(\frac{1}{\bar{\gamma}+1}\right)}\right). \tag{2.74}$$

Constants A and B in Equations (2.72), (2.73), and (2.74) are experimentally-determined electron impact ionization constants, available in Raizer.[21] In Equation (2.74), the constant $\bar{\gamma}$ represents the secondary emission coefficient. Secondary emissions occur at voltages near breakdown and amplify the ionization effect. These emissions can be caused by positive ions that shed electrons, photons, and metastable atoms.[42] The breakdown voltage in Equation (2.72) depends on the product of pressure p and distance between electrodes d. The voltage can be plotted versus the quantity pd, giving a curve of ignition conditions. These experimental curves of breakdown voltage are called Paschen curves, and are a useful tool for determining the optimum ionization conditions.

In the case of microwave breakdown in a resonator cavity, like in an MET, the quantity d is not easily defined. Instead, a diffusion length Λ is taken into account. The diffusion length comes from the size of the resonator cavity, and represents a distance that an electron can be expected to travel before hitting cavity walls and potentially recombining with ions there. The diffusion length depends on the radius and length of the cavity, and frequency of the electric field variation. Considering the diffusion length within a resonant cavity, the breakdown field condition becomes[21]

$$\frac{E_t}{p} = \frac{\text{const}}{\text{const}' + \ln p\Lambda}. \tag{2.75}$$

Equations (2.75) and (2.73) are very similar because d and Λ both characterize the removal of electrons from their respective systems. As a result, experimental plots of breakdown electric field versus cavity pressure at different frequencies and diffusion lengths can be made, similarly to Paschen curves, which show optimum breakdown conditions.

2.4 Small Spacecraft Overview

2.4.1 Small Spacecraft Issues

Small spacecraft have become more popular in recent years due to their lower costs and shorter development times over large traditional spacecraft. However, due to their size, small spacecraft face a number of issues that are unique from larger spacecraft. The smaller size and limited resources lend themselves to a tradeoff in functionality, and it is the goal of further research into miniaturization to remove these negative tradeoffs.

Power systems are a significant barrier to expanding small spacecraft functionality. Traditionally, spacecraft are powered by solar cells directly and that charge batteries. Limited surface area puts a hard restriction on the amount of power than can be generated. Current state-of-the-art commercially available deployable solar panel systems are able to produce about 50 W for a 3U CubeSat using about 30% efficient triple-junction cells. Advanced lithium–ion batteries used for storage aboard spacecraft have energy densities of around 200 W·h/kg. As solar technologies improve, they will allow for more available power in smaller packages. Performance of power systems also supports other aspects of spacecraft operation. Command and data handling, as well as communications aboard small spacecraft, are often limited by the available power. Development of novel power options, such as miniature radioisotope thermal generators, may also increase power performance.[22]

Propulsion systems currently used for small spacecraft are not very sophisticated, but a number of projects are tackling this area of research. All CubeSat-scale propulsion systems are constrained by the same factors. A lack of volume inside the craft provides limited options for propellant storage and packaging of thruster components. Propellant is often pressurized, which also poses a problem for CubeSats, which are regulated to protect primary payloads during launch. Small amounts of available power is also a problem because valves and other electric components can be very power-hungry. Improvements to small propulsion systems are sure to come soon, though, as this relatively young field matures. For example, the introduction of MEMS-based devices can significantly reduce power consumption and size of propellant system components like valves.[22]

Spacecraft attitude determination and control systems are often critical to accomplishing the intended mission. Attitude thrusters and momentum wheels are not common on small spacecraft due to large amounts of resources they usually require. Pointing accuracy depends on precise instruments as well, which is substantially more difficult to accomplish on smaller craft.

CubeSat pointing accuracy is currently around 2°, but future research into miniaturized star trackers, attitude control equipment, and software should see pointing accuracy increase. Tracking accuracy for 100-kg spacecraft has the potential to become more accurate than 0.1° through development of small attitude thrusters.[22]

Thermal control is very important for spacecraft of all sizes. There are generally two types, passive and active thermal control. Passive thermal control is ideal for small spacecraft because elements like thermal coatings or insulation do not require power and take up very little room. However, active thermal control is more effective with the tradeoff of requiring more power and space. Equipment such as radiator thermal loops cannot be made effectively for small spacecraft. Battery cooling or thermal control of sensitive equipment like cameras can increase the effectiveness of those components. In the future, active thermal control will be necessary to expand the mission capabilities of small spacecraft.[22]

Deploying small spacecraft also poses unique challenges. Currently CubeSats have a number of possible options for deployment. The P-POD is the most common launch adapter. Integration through the Naval Postgraduate School's CubeSat Launcher (NPSCuL) or being deployed from the ISS are also possibilities. In all these situations, however, CubeSats are the secondary payload, which puts them at the mercy of the primary payload. Because of this, CubeSats have limitations on their possible orbits and, in turn, limitations on possible science missions. Launching along with bigger missions also takes away from a major benefit of small spacecraft. Working around schedules of large launch vehicles can increase iteration time and costs associated with development.[22]

2.4.2 CubeSat Overview

The goal of current MET projects is to create a thruster for the CubeSat bus standard. The CubeSat standard was developed for very small satellites by California Polytechnic State University, San Luis Obispo, and Stanford University's Space Systems Development Lab in 1999.[23] It was originally developed as a teaching tool to give students hands-on experience with practical space systems projects. Since then, many small-to-large private corporations and NASA have used CubeSats for their own small-scale missions and experiments.

CubeSats are most commonly classified by their size, measured in units (U). One U consists of a single 10-cm cube.[24] Larger satellites can be classified along the lines of 2U or 3U, which are CubeSats consisting of two and three stacked 10-cm frames, respectively. In recent years, larger configurations of up to 6U have been considered for more demanding missions, including potential interplanetary applications.[23] The standard specifies that a typical 1U CubeSat must have a mass of no more than 1.33 kg.[25] Average power consumption is generally on the order of a few watts, and available data rates cannot exceed 1 Mbps.[25] CubeSats can be designed and launched for costs ranging from $50,000–200,000,[25] which are significantly lower than traditional satellite missions. The CubeSat standard encourages use of low-cost and commercial-off-the-shelf (COTS) components to drive the price down.

An important feature of CubeSats is a standardized launch platform called Poly-Picosatellite Orbital Deployer (P-POD). A P-POD consists of a simple spring-loaded aluminum box that can store and eject a number of CubeSats that add up to 3U in size.[26] The P-POD simplifies the launching a CubeSat by eliminating the need to design a deployment system. The deployer is designed to interface with larger launch vehicles and can be launched as a secondary or tertiary payload such that it does not interfere with the primary payload. P-POD also protects the satellites *en route* to orbit, as well as facilitates proper ejection and separation of the satellites in order to prevent interference from each other or remains from the launch vehicle.

The first set of CubeSats were launched in 2003.[26] The set consisted of two P-PODs with four satellites. All of these satellites were developed primarily by universities. The launch and deployment were successful, and all satellites were confirmed to have made it to orbit. The most notable satellite deployed with this launch was the geological science mission QuakeSat, which provided data for early detection of earthquakes. The most recent launch occurred in June 2014, on which three CubeSats were released in orbit during the Dnepr UniSat-6 mission.[27] Many more launches are planned for 2015 and beyond.

2.4.3 CubeSat Propulsion Overview

To date, there have been only a handful of CubeSat missions with propulsion systems onboard. The first CubeSat to feature a propulsion system was the CanX-2.[25] It was developed by the University of Toronto Institute for Aerospace Studies Space Flight Laboratory (SFL) and launched in 2008. The 3U CubeSat carried a cold-gas Nano Propulsion System (NANOPS).[28] This module used sulfur hexafluoride (SF_6) propellant, which achieved a maximum thrust of 35 mN, an average specific impulse of 46.7 s, and was estimated to deliver a total ΔV of about 35 m/s. The whole module weighed less than 500 g. NANOPS and the CanX-2 mission served as a technology demonstration for later, more advanced projects, such as the CanX-4/5. This pair of identical nanosatellites launched in late 2014 and demonstrated formation flying using a propulsion system similar to NANOPS.[29]

The Delfi-n3Xt 3U CubeSat launched by the Delft University of Technology in November 2013 included a cold gas thruster as well.[30] This module had a mass of 119 g and used nitrogen, stored as a solid, for propellant. The system achieved a thrust of 6 mN and a specific impulse of about 30 s. The satellite was primarily used to demonstrate propulsion technology and for radio experiments.

Electric propulsion has not been demonstrated yet in space on a CubeSat mission. A Vacuum Arc Thruster (VAT) module was to be flown on the ION CubeSat in 2006.[25] Unfortunately, due to launch vehicle failure, the satellite was lost. The VAT was estimated to have a specific impulse of about 1000 s.

While there is a lack of flight-tested propulsion options for CubeSats, there are also many research projects into small spacecraft propulsion systems that aim to be incorporated into CubeSats or other similar-sized spacecraft. Cold gas thrusters are a popular proposed design because of their simplicity. Some designs, such as the JPL hydrazine MilliNewton thruster,[31] are based on miniaturized versions of established technologies. This thruster has all the same parts as traditional hydrazine thrusters, including valves, catalyst bed, and piping, but is much smaller. Hydrazine thrusters may not be a practical choice for universities, but it is a possible propellant for government and commercial applications. Similar cold gas thrusters can also operate using other propellants. For example, Moog produces many miniature nitrogen (N_2) thrusters that are safer for handling.[32] Unfortunately, many miniature cold gas thrusters such as these that were not specifically designed for CubeSats require power for their valves that exceeds most CubeSat power budgets. There are also concerns about pressurized propellant tanks, since the standard limits allowed internal pressure.

One of the solutions to problems with power usage is microelectromechanical systems (MEMS) technology. Valves based on MEMS generally require less power than traditional solenoid valves. For example, a MEMS-based butane cold gas module developed by NanoSpace has been flown on the European PRISMA satellite.[33] This propulsion system was contained in a 10 cm × 10 cm × 3 cm space and provided around 15 m/s of ΔV. It used an average of 2 W per thruster and had a total of four thrusters. The butane was stored as a liquid, allowing the module to keep its propellant at a relatively low pressure. The module is to be adapted for CubeSat use with plans to implement it on upcoming European QB50 project CubeSats.[33]

To solve the pressure problem, some designs have used solid propellant storage. The European Delfi-n3Xt satellite mentioned previously stored its nitrogen propellant as a solid. Its propulsion system, dubbed $T^3\mu PS$, was developed through collaboration between Dutch organizations TNO, Delft University of Technology, and University of Twente. The module consists of a MEMS valve and nozzle, Cool Gas Generators (CGG) for nitrogen storage, a plenum for nitrogen expansion once it is converted to its gaseous state, and a printed circuit board containing electronics for module operation.[34] This design allows propellant to be stored at a low pressure and uses low power, requiring only about 2.5 W for operation.[32] However, as all cold gas thrusters, $T^3\mu PS$ has a low efficiency and a low ΔV compared to other thruster designs.

An alternate to pressurized or solid storage is liquid propellant storage. Some propellants, such as butane or ammonia, can be stored as liquids that transition into gases upon expansion. One example of this design is the NanoSpace thruster mentioned above, but some other well-developed thrusters of this type come from VACCO Industries. In collaboration with JPL, VACCO developed a series of miniature thruster technologies, including its own Chemically Etched Micro System (ChEMS) technology, for NASA's Micro-Inspector spacecraft concept.[35] This experience later lead to the development of VACCO MEPSI micro propulsion system.[32] The module is commercially available specifically for 1U CubeSats and is designed to operate using stored liquid isobutane propellant. MEPSI can provide 53 mN of thrust at 70 s specific impulse for a total of 34 m/s ΔV. VACCO also offers an alternate module, the Palomar micro propulsion system developed in collaboration with Boeing.[36] This larger system is meant to be used on 3U CubeSats and can provide 35 mN of thrust.

For improved thruster performance, some proposals use "hot" chemical thrusters that heat the propellant for a higher exhaust velocity. The simplest type of chemical thruster is a solid rocket. Because the propellant is solid, a limited number of support systems are required. There is no need for valves or piping, so packaging and integration are easier than with more complicated systems. On the other hand, solid rockets generally cannot be throttled, turned off once ignited, or restarted. They tend to provide a large thrust and acceleration, which may be unnecessary for CubeSat applications. Therefore, solid rocket options for small satellites are limited. ATK is one company that provides solid rockets for small satellites. Their STAR series motors are small enough to potentially be integrated on a CubeSat, although they were not explicitly developed for this purpose. An ATK STAR 5A motor produces 169 N of thrust at a specific impulse of 250 s.[32] A motor like this could provide 1.3 km/s ΔV to a 1U CubeSat with 4 g acceleration.

A more novel application of solid rockets to CubeSats could be in the form of digital microthruster arrays. A number of research groups from government agencies, like NASA Glenn, private industry, like Aerospace Corp. and Honeywell, and universities, like Caltech, have all participated in digital propulsion projects.[32] Overseas teams from LAAS in CNES in France and KAIST in South Korea have run similar projects as well.[32] All digital thruster arrays work in a similar fashion. An array consists of micromachined wafer layers that hold a large number of very small igniters, propellant cavities, and nozzles. These cavities can be ignited individually or in bulk, depending on thrust requirements at the time. One cavity ignition may provide a very small impulse, but a large number of them can provide significant thrust if needed. Currently, no such devices have been flown on CubeSat missions, and there are generally issues with precise control of ignition.[32] In the future, digital microthruster arrays can provide simple and easily integrated propulsion to CubeSats and other small satellites.

Bipropellant thrusters are common for large space vehicles, but are hard to execute in small satellites. In addition to potentially complicated piping systems, there is also a need for two separate propellant tanks, which are very limited by available volume inside a satellite like a CubeSat. Due to these factors, bipropellant propulsion systems for CubeSats are not common.

One notable project is the HYDROS thruster by Tethers Unlimited, Inc.[37] This device is being developed specifically for CubeSat use. It is novel in storing its propellant as water and then splitting it through electrolysis into oxygen and hydrogen gasses, which are then combusted to provide thrust. The thruster is still undergoing development, but the project hopes to deliver up to 0.8 N of thrust at 300 s specific impulse for a total of 100–300 m/s ΔV for a 3U CubeSat.[37] TUI hopes to achieve TRL-6 in 2015.

Electric propulsion is a very attractive option for small satellites like CubeSats. Electric propulsion devices usually have a high specific impulse, allowing for reduced propellant mass. Thrust produced by electric systems is generally low, but this is suitable for a large number of small satellite missions. There are many electric propulsion projects under way, with many different electric systems.

Pulsed plasma thrusters (PPTs) have a long heritage of space flight, starting as far back as the 1960s. These devices work by creating an electric discharge between two electrodes, which then ablates a solid fuel rod. The ablated material is accelerated due to Lorentz forces.[32] There have been a number of attempts to miniaturize PPTs for small satellites. In one of the most notable attempts, Busek Company, Inc. helped develop and flight test a PPT on the FalconSat-3 satellite in 2007.[38] FalconSat-3 was a small satellite, but not a CubeSat, and the company has since then been using its experience to create a dedicated CubeSat PPT module, to be released in the near future.

Vacuum arc thrusters (VATs) are another type of electric propulsion common to small satellites. Their operational principle is similar to PPTs; however, the ablated material comes from erosion of the electrodes themselves.[32] VATs are inherently compact because they do not need a separate propellant storage volume, so they are very attractive for CubeSat use. VATs were originally developed by Alameda Applied Sciences Corporation (AASC).[32] The ION mission mentioned previously was equipped with a VAT developed in collaboration with AASC and intended for flight testing.[25] VATs will likely see more use soon, as a number of groups have been investigating their use on CubeSats, especially for formation flying experiments. For example, the European UWE-4 CubeSat is being designed with a plan to incorporate this type of thruster.[39]

Ion thrusters are another type of electric propulsion with a long heritage of space flight. Ion thrusters operate by ionizing a propellant and accelerating it through an electric field. This type of thruster has been used on many satellites, including some small satellites. There has not been a flight-tested version of an ion thruster designed for CubeSats; however, there have been a number of attempts to miniaturize the technology for this purpose. One of these attempts comes from Penn State. The Miniature Microwave Ion Thruster (MMIT) and the Miniature Radio-Frequency Ion Thruster (MRIT) were developed at Penn State starting in the mid 2000s.[40] The latest version of the MMIT thruster is about 1 cm across, and further research efforts will try to improve thruster performance, especially power requirements, with the ultimate goal of incorporating it on a small satellite, such as a CubeSat.

Hall thrusters are electrostatic propulsion devices that are in a similar position to ion thrusters. They have some heritage of being flown on larger missions, but attempts at miniaturization have not yet yielded a thruster suitable for CubeSats. For example, a miniature Hall thruster developed at MIT was only 4 mm in diameter and delivered 1.8 mN of thrust at 826 s specific impulse.[34] However, effective operation required 126 W of power, which is unrealistic on a CubeSat.

One of the less common types of miniature thrusters available today are electrospray thrusters. These are also electrostatic devices, but they do not require plasma like ion or Hall thrusters. Mature electrospray technologies exist today and have been flown on larger satellites. One of these is the Busek Co. electrospray thruster developed for the NASA-ESA joint Lisa Pathfinder mission. Following on this work, Busek is developing a miniature thruster for CubeSat use that will use only 0.5U of volume.[41] Similarly, a number of projects into miniature electrospray thrusters are currently ongoing, but are not ready for CubeSat integration yet.[32]

Resistojets are another notable electric propulsion technology, and is actually the simplest of all. A resistojet simply uses an electric heat exchanger to heat up a propellant before it is expelled from a nozzle. Resistojets offer only slight performance improvements over cold gas thrusters, but their simplicity can be attractive for some missions. Resistojets tend to use a lot of power, and are therefore usually unsuitable for CubeSats. However, Busek offers an ammonia micro-resistojet which consumes 1U of space and less than 15 W while providing 60 m/s ΔV at 150 s specific impulse.[42]

Some even more exotic propulsion options do not require any propellant at all. Electrodynamic tethers are one example of propellantless propulsion. These tethers simply take advantage of Lorentz forces due to moving electrons within very long conducting strands that can be deployed from the spacecraft. A number of technology-demonstration missions for this type of propulsion have been carried out, including the Multi-Application Survivable Tether (MAST) CubeSat (which was not a conducting tether).[32] Another propellantless technology being explored for CubeSat use is solar sails. Solar sails work by transferring momentum from the Sun’s photons to the spacecraft. This is a niche technology because solar sail can only be useful when the spacecraft is at a certain orientations and very low thrust is required. However, this option is still being researched. For example, the NASA Nanosail-D 3U solar sail demonstrator mission was launched in 2010 as payload on the FASTSAT mission.

Chapter 3

Thruster System Design

3.1 Design Objectives

The current 17.8-GHz MET prototype is a test model for laboratory use. Its design had to approximate a flight-ready thruster as closely as possible, while allowing for ease of testing in the laboratory.

Most importantly, the thruster cavity was designed to resonate in the TM^z_{011} mode and operate in the K_u microwave band. The TM^z_{011} mode was chosen because previous MET experiments showed this to be the optimum mode for plasma formation near a nozzle in the cavity. The K_u microwave band was chosen to allow access to a greater range of COTS parts than what is available for higher-frequency bands. The K_u band includes frequencies from 12 GHz to 18 GHz, so a target frequency of 17.8 GHz was selected in order to remain in the band while making the thruster as small as possible.

Size was a driver because of the eventual goal of including an MET on a CubeSat. A CubeSat thruster must be very small. In addition to physical size, having a high resonant frequency has the effect of creating higher electric field concentrations within the cavity, allowing plasma to light at lower input power values. The 17.8-GHz cavity was designed with the objective of achieving plasma ignition with input powers of 10 W or less.

The test thruster design also had to include a way to confirm plasma ignition. Just as with previous designs, the 17.8-GHz cavity incorporates a viewport centered on the upper half of the cavity near the nozzle in order to visually identify plasma formation. As a note, the viewport would generally not be on a flight version of the thruster.

Previous MET tests showed that plasma ignition is easiest to achieve at low pressures. Some tests must be done outside a vacuum chamber, so the cavity was designed to be able to maintain a partial vacuum while a pump vacates the cavity through the nozzle. The cavity must also prevent propellant from leaking. The propellant ports were designed to allow the incoming propellant to form a vortex. The vortex helps stabilize the plasma inside the cavity once it is lit.

3.2 Thruster Design Overview

The most important part of thruster design is sizing of the cavity. The size of the cavity determines the resonant frequency and resonant mode at which the MET will operate. Equation (2.64) provided the starting point. The chosen dielectric was quartz due to its ready availability. The thickness of the dielectric, t, was chosen to be 1/16 inch, because this was the smallest commonly available quartz disk thickness. Based on calculations using this equation, a height of 21.1 mm and cavity radius of 6.8 mm for the desired resonant frequency of 17.8 GHz were calculated, assuming a height-to-radius ratio of about 3.1. The ratio was chosen because of its demonstrated effectiveness in previous MET models. These dimensions were further confirmed via COMSOL Multiphysics simulations.[43] The cavity was also sealed by O-rings to keep control of internal pressure.

Once the cavity dimensions were selected, the rest of the thruster head was designed to support the power and propellant systems. The antenna was chosen based on COMSOL Multiphysics simulations, comparing SMA, SSMA, and 2.4-mm candlestick connectors. The 2.4-mm candlestick showed the strongest electric fields within the cavity.[43] The pressure tap and viewport grid sizes were chosen based on their machinability with commonly available drill sizes small enough to not cause significant electromagnetic interference within the cavity. The viewport hole diameters could be no more than 1/20 of the wavelength.[5] For the 17.8-GHz cavity, that means that no holes with a diameter greater than 0.033 inches could be made in the sides. The propellant ports were made using the smallest available drill diameter, 0.0059 inches, in order to increase the propellant velocity within the chamber to ensure the formation of the propellant vortex. The ports were placed tangentially to the walls and as close as possible to the nozzle. The nozzle was made using the same diameter drill as the propellant ports to increase exit velocity. The nozzle was straight and without any converging or diverging portions because a complex nozzle would be difficult to manufacture on this scale, and this was outside the scope of the project.

The large outer dimensions of the thruster head, despite a small inner cavity, were due to a need for large flat surfaces that Swagelok fittings in the propellant ports could seal against with O-rings. The bolt sizes for the hardware that held all the MET plates together were chosen based on availability. The antenna bolts were specified by the manufacturer, and it was practical to reuse the bolt size for the nozzle plate and viewport plates, since those were also very small components. All the thruster head parts can be seen below.

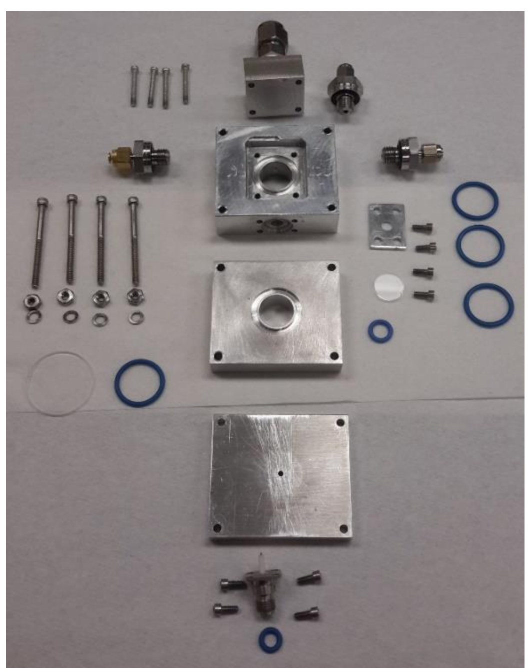

Figure 3.1: 17.8-GHz MET thruster head components

In the final configuration, propellant ports could not be machined as planned in the design. Commercially available drill bits for the final port diameter were not available in lengths that allowed for drilling straight though from the outside to the cavity. An intermediate step had to be implemented, in which a small bolt was threaded partway into the port. The bolt was drilled through the center, and a length of stainless steel hypodermic tubing with a final inner diameter of 0.006 inches delivered propellant to the cavity.

Figure 3.2: Propellant port bolt

The completed 17.8-GHz MET thruster head can be seen in Figure 3.3 below.

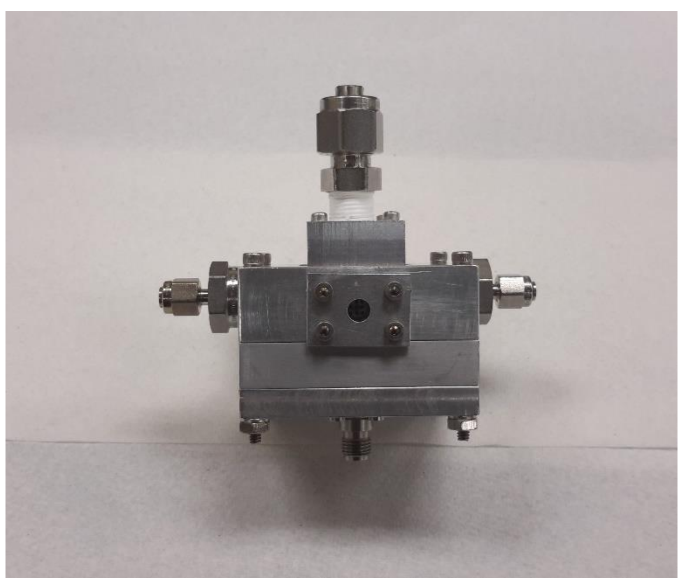

Figure 3.3: Head on view of assembled MET thruster head

3.3 Antenna Height Optimization

For optimum operation, the MET cavity must have high coupling efficiency. A high coupling efficiency means that more of the power transmitted into the cavity via the antenna is absorbed by the propellant inside instead of being reflected. Coupling efficiency can be described using the following equation[16]

$$\text{Coupling Efficiency (\%)} = \frac{P_{\text{for}} - P_{\text{ref}}}{P_{\text{for}}} = \frac{P_{\text{inp}}}{P_{\text{for}}}. \quad \textbf{(3.1)}$$

Coupling efficiency depends heavily on antenna height, which refers to the distance that the candlestick antenna at the bottom of the cavity protrudes into the cavity. A number of COMSOL Multiphysics simulations have been done by previous researchers on thrusters with various resonance frequencies to determine the optimum antenna height. Simulations by Sinha[43] focused on cavity dimensions used by the 17.8-GHz MET. The results, shown in Figure 3.4, are similar to those from all previous simulations. Antenna height close to 0 mm, or flush with the bottom surface of the cavity, is best for electric field intensity, and, by extension, coupling efficiency.

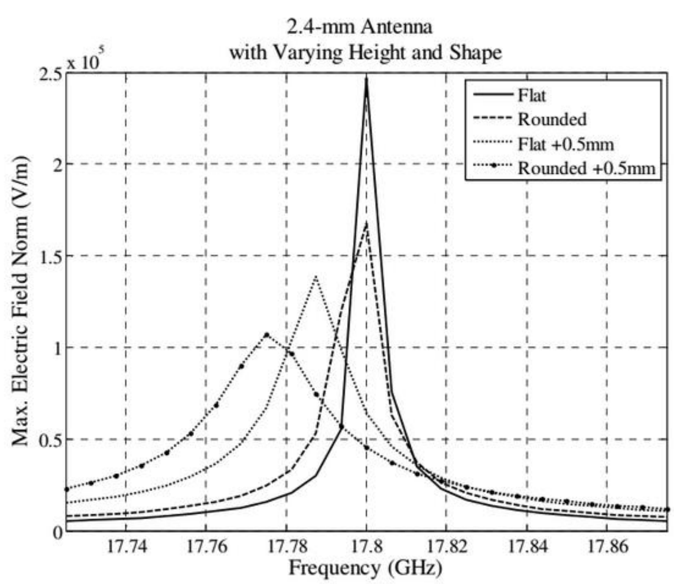

Figure 3.4: Antenna height optimization for 17.8-GHz cavity with a 2.4-mm antenna[43]

To confirm this prediction, the resonant cavity was placed on a network analyzer and S_{11} mode measurements were made. Antenna height was varied by carefully filing down the conductor of the candlestick, keeping the tip as flat as possible. The height above the antenna plate was measured using calipers and the resultant resonant frequency and reflected power were observed on the network analyzer. The resonant frequency varied throughout the process, starting at 17.8 GHz and increasing to 17.98 GHz as antenna height decreased. The reflected power results are in Figure 3.5 below.

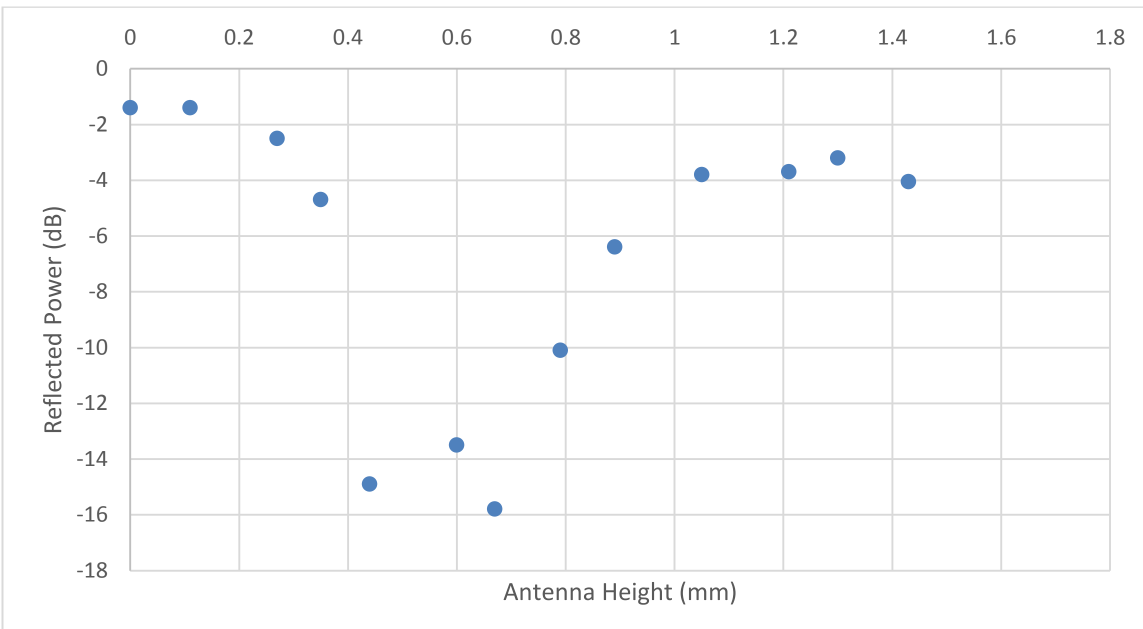

Figure 3.5: Variation of reflected power with antenna height of 1.43 mm to 0 mm above antenna plate

Experimental results did not completely agree with simulations. The reflected power went down until a height of 0.67 mm, but then rapidly increased. The reflected power of −1.4 dB for a flush antenna was even higher than −4.05 dB for an unmodified one. A second antenna was modified in the same manner using experimental results as a guideline. The result can be seen in Figure 3.6. The reflected power for this second antenna was never as low as the test case, but due to the apparent sensitivity of the cavity to antenna height around the optimum height region, no further attempts at modification were made. The final antenna height used for hot fire tests was 0.72 mm, corresponding to a reflected power of −9.9 dB and 17.92 GHz resonant frequency.

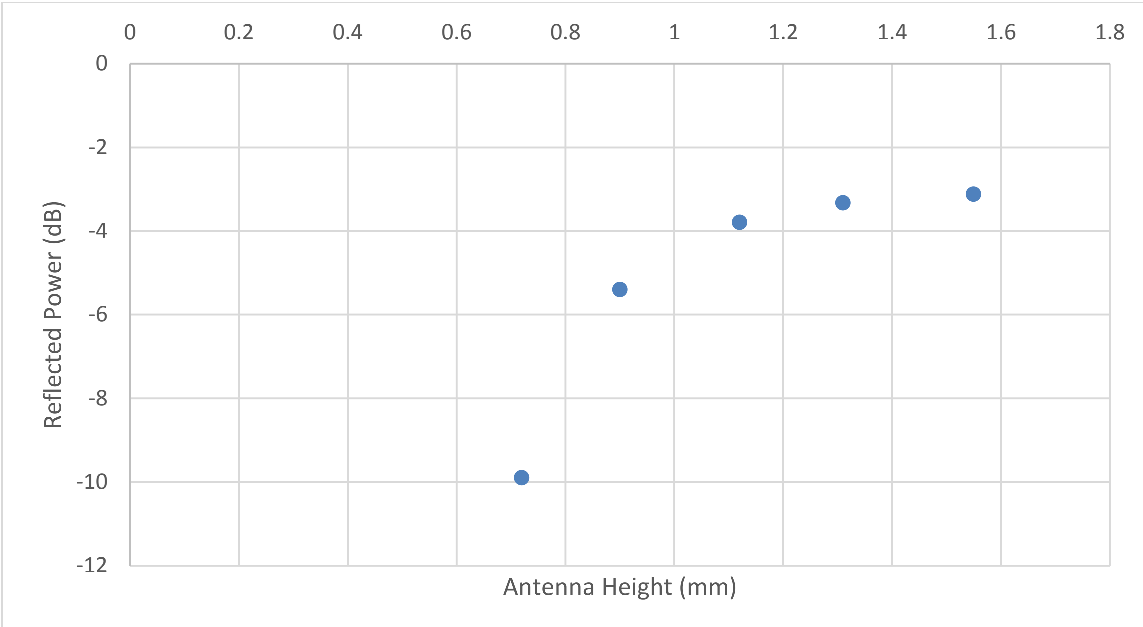

Figure 3.6: Variation of reflected power with antenna height used for thruster head tests

3.4 Design Guidelines for CubeSat Propulsion System

The 17.8-GHz thruster head was designed with the understanding that the final product is to be a part of a complete propulsion system aboard a CubeSat. The requirements and restrictions of the CubeSat standard dictate the design guidelines. Previous work analyzed the CubeSat propulsion module using systems engineering principles to develop a set of requirements.[44]

The first set of requirements deals with limitations imposed by the CubeSat standard itself. A CubeSat propulsion system must meet the following criteria (assuming 1 U):

- 1 liter volume
- 1.33 kg mass
- Contained within 1U envelope

- Meets NASA Launch Services Program (LSP) requirements for CubeSats

In addition, to make the propulsion system effective in fulfilling mission needs, the following performance guidelines are desirable for the module as a whole:

- No more than 50 W total power
- 500 m/s ΔV
- Relighting ability
- 0–60 °C temperature range

The CubeSat propulsion module can be separated into four distinct subsystems. The first is the thruster head subsystem, second is the power subsystem, and third is the microwave source subsystem, and finally the propellant subsystem. The requirements for the thruster subsystems include guidelines for the MET cavity itself.

- Up to 3 mg/s mass flow
- Up to 10 W delivered microwave power
- Ammonia propellant
- 17.8 GHz ±75 MHz resonant frequency

The thruster requirements are derived from experimental performance of past thrusters. The frequency range gives the thruster head desirable physical size, whereas the propellant mass flow and power requirements are realistic expectations for a system that can be sustained on a CubeSat. Ammonia is the preferred propellant for this system because experiments with past METs showed high specific impulses using this propellant. Ammonia is also storable as a liquid at around room temperature, which allows for more propellant to be stored in a small tank. Ammonia is considered a green propellant by NASA because of its low toxicity compared to propellants like hydrazine. Following NASA's green propellant guidelines is another goal for the propulsion system.

The power subsystem is meant to provide power to all electrical components in the propulsion module. The subsystem must:

- Handle and distribute up to 50 W
- Provide 33 W at 40 V and 825 mA to microwave source subsystem
- Provide 6 W at 24 V and 250 mA to propellant subsystem
- Must respond to command signals from satellite mission payload
- Protect module and CubeSat from overcurrent

The maximum power available to a CubeSat using state-of-the-art solar panels is about 50 W. The power allocation amounts are based on estimates for power requirements for components in subsystems that the power subsystem interfaces with. The microwave source subsystem needs a lot of power to run the microwave generator and the amplifier, and the propellant system needs power for electric valves and heaters to vaporize propellant. The power subsystem must also be controlled to produce thrust on demand and keep the module and CubeSat safe from power-related failures.

The microwave source subsystem is responsible for producing and delivering microwave power for plasma ignition. The requirements for this subsystem include:

- 17.8 GHz fixed frequency with ±75 MHz tuning ability
- 40 W maximum input power
- 10 W microwave power delivered to thruster
- Microwave source and amplifier in one package
- Source and amplifier combined maximum mass of 200 grams
- Arranged to use excess heat from microwave components to aid in propellant vaporization

The microwave source requirements are derived from the needs of the resonant cavity and the available resources from the CubeSat. The frequency requirement has to support the cavity resonant mode, and the delivered power is necessary to achieve plasma ignition. Maximum power used by the subsystem is restricted by total power generated by the CubeSat itself. The physical requirements stem from the size and mass limitations of the CubeSat standard.

The propellant subsystem acts to store and deliver propellant to the thruster cavity. The subsystem consists of at least three devices: the propellant tank, the tank valve, and the propellant vaporizer. The propellant tank has the following requirements:

- 1 kg maximum
- 550 cm^3 volume minimum
- Store 360 grams of ammonia at up to 500 psi

The mass requirement comes from the CubeSat standard. The tank volume was calculated from the amount of ammonia necessary to produce the necessary amount of total ΔV. The maximum pressure is derived from ammonia's vapor pressure at the maximum temperature that the CubeSat would be expected to reach with an added margin of safety. Following the tank, the valve has the following requirements:

- 5 W maximum
- 100 grams maximum
- 2 inches maximum length, 1 inch maximum width
- 500 psi maximum operating pressure
- Stainless steel body for ammonia corrosion resistance
- Flow rate range of 0.5 mg/s to 3 mg/s

The valve's operating pressure must be in line with the worst-case scenario experienced by the propellant tank. The physical dimensions of the valve have to be minimized because of

CubeSat space restrictions, and it must be built to handle ammonia, which can be corrosive to some materials. The valve must use as little power as possible, with no more than 5 W to be allocated to it. The flow rate has to be within the stated parameters, which will be narrowed down when flow rate for optimum thrust is experimentally determined in future work.

The final component of the propellant subsystem is the propellant vaporizer. Ammonia can be stored as a liquid, but the MET requires a gas to ignite plasma. The propellant subsystem must be able to handle liquid ammonia and convert it to a gaseous form before it reaches the thruster. The ideal vaporizer would have a mass of no more than 100 g. It may use small heaters, porous metal inserts in the propellant lines, and the natural pressure drop of the system to achieve its goals. Further design and experimental work will be needed to determine the final vaporizer design.

Chapter 4

Experimental Setup and Test Results

4.1 Setup Overviews

4.1.1 Experimental Setup for Tests with Helium as Propellant

After the thruster head itself was designed and manufactured, the rest of the supporting systems for running the thruster were assembled. These initial tests used benchtop lab equipment, which would not be used for tests simulating operation on an actual CubeSat.

The thruster needed a microwave power and propellant system. The microwave signal generated using an HP signal generator, which was fed into a Xicom traveling wave tube amplifier (TWTA) to increase power level. The TWTA had a waveguide output, which was converted into SMA coaxial cable, and finally connected to the antenna on the thruster head via an SMA-to-2.4-mm transition.

The helium propellant was supplied by a pressurized gas cylinder. This tank was connected to a Tylan flow controller, which was operated by a Unit Instruments flow controller power supply. The flow controller output was split into two lines using a tee-fitting. The two lines were connected to the two port fittings on the sides of the thruster head. An Omega pressure transducer was connected to the pressure tap fitting in the thruster head, and its readout was monitored through an Omega process panel meter. Attached to the nozzle of the MET thruster head was a vacuum line connected to a Leybold vacuum pump. The pump was situated inside a fume hood for venting of exhaust. There were two valves in line with the vacuum attachment, which allowed the pump to be isolated and the MET to vent directly to atmosphere. This feature was used to protect the pump when the thruster head was operated under high-pressure conditions. The propellant lines leading into the MET were all made out of clear PTFE tubing and Swagelok fittings. The vacuum line leading to the pump was opaque nylon tubing. A detailed parts list and block diagram of this setup is shown in Figure 4.1.

Testing was initially done using an Omega PX303-050A5V pressure transducer. However, partway through testing, the transducer seems to have been damaged, and so remaining data was gathered using an Omega PX178-100S5V.

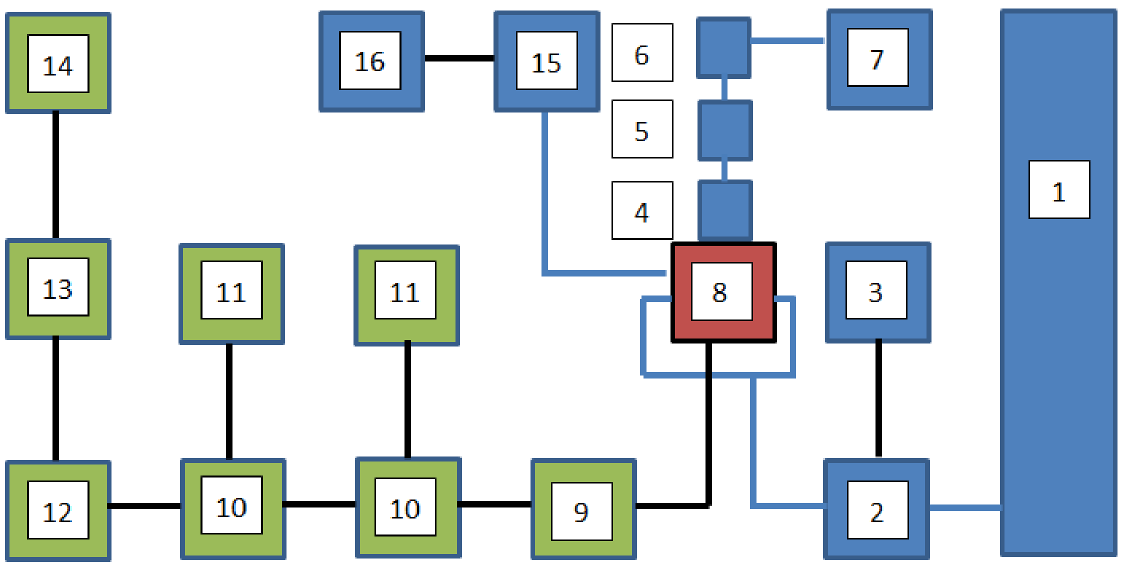

Figure 4.1: Schematic for experimental setup for MET ignition tests with helium as propellant

1. Helium tank
2. Tylan FC-2900V flow controller
3. Unit Instruments URS-20 flow controller power supply
4. Bolted vacuum nozzle attachment
5. Atmosphere venting hand valve
6. Pump cutoff hand valve
7. Leybold Trivac D4A vacuum pump
8. Microwave electrothermal thruster head
9. Rosenberger SMA to 2.4-mm coaxial transition
10. Narda 4016C-20 coaxial directional coupler
11. Agilent 8481A power sensor
12. E&M Laboratories KU130LI waveguide isolator
13. Xicom Technology XTRD-270DBSR TWTA

14. Hewlett-Packard 8671B Synthesized CW Generator
15. Omega PX303-050A5V pressure transducer
16. Omega DP25-E-A process panel meter

4.1.2 Experimental Setup for Tests with Ammonia as Propellant

The microwave power components of the setup remained the same for tests with ammonia as they were for helium propellant. The same TWTA, signal generator, and power sensors were used and in the same configuration as described in Section 4.1.1.

The propellant systems for operating the thruster with ammonia had to be modified to account for ammonia's very different properties from helium. Because of ammonia's more reactive nature, it had to be ensured that all components were made out of aluminum, stainless steel, and ammonia-safe polymers like nylon and PTFE. No brass fittings or transitions could be used because their integrity would be compromised when in contact with ammonia. Ammonia is also mildly toxic if allowed to contact human skin or inhaled, so extra effort went into ensuring there were no leaks in the system and that all exhausts were safely vented under a fume hood. The propellant system was also set up in such a way that both helium and ammonia propellants were connected at the same time and could be switched at will.

An ammonia tank was connected to a Unit Instruments flow controller, designed and calibrated specifically for use with ammonia. This flow controller was separated from the rest of the system with a hand valve to allow the flow to be completely cut off when ammonia was not being pumped into the thruster cavity. The valve was connected to a tee-junction, which lead to both the thruster cavity and the helium branch of the propellant system. The helium branch of the propellant system was configured in the same way as the ammonia system, except with the same Tylan flow controller that was used in previous helium tests. A more detailed diagram of all the components and their arrangement can be seen in Figure 4.2.

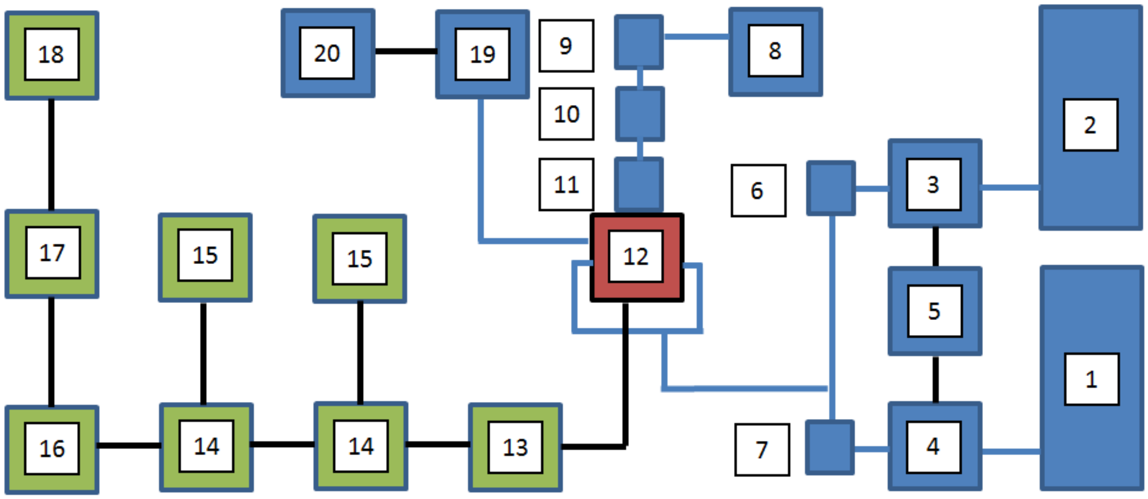

Figure 4.2: Schematic for experimental setup for MET ignition tests with ammonia as propellant

1. Helium tank
2. Ammonia tank
3. Unit Instruments, Inc. UFC-1660 flow controller
4. Tylan FC-2900V flow controller
5. MKS Instruments 647B multi gas flow meter
6. Ammonia cutoff hand valve
7. Helium cutoff hand valve
8. Leybold Trivac D4A vacuum pump
9. Pump cutoff hand valve
10. Atmosphere venting hand valve
11. Bolted vacuum nozzle attachment
12. Microwave electrothermal thruster head
13. Rosenberger SMA to 2.4-mm coaxial transition
14. Narda 4016C-20 coaxial directional coupler
15. Agilent 8481A power sensor
16. E&M Laboratories KU130LI waveguide isolator
17. Xicom Technology XTRD-270DBSR TWTA
18. Hewlett-Packard 8671B Synthesized CW Generator
19. Omega PX178-100S5V pressure transducer
20. Omega DP25-E-A process panel meter

4.2 Operational Procedures

4.2.1 Cold Flow Procedure with Helium as Propellant

Cold flow tests were performed to establish the range of pressures within the resonant cavity caused by a corresponding range of mass flow rates. This relationship is crucial to plasma ignition, as each particular pressure requires a certain amount of power to achieve electric breakdown. Therefore, propellant mass flow rate can be related to ignition power.

Before the testing could begin, the atmosphere vent valve had to be closed and the pump cutoff valve had to be open. The helium tank valve was opened, and the regulator valve was open enough to reach 60 psi of pressure in the regulator. The Leybold vacuum pump was turned on and the pressure inside the cavity was allowed to reach a steady minimum, as indicated by the Omega pressure transducer. The flow controller was operated though a Unit Instruments flow controller power supply. The power supply could be set to any number in a range of 1 to 100, which indicated the percent of maximum flow rate allowed by the flow controller. Once the steady minimum pressure in the cavity was achieved, the power supply was set to the desired flow rate. The pressure was allowed to reach a steady reading for about 30 seconds. The flow rate could then be adjusted, and the new resulting pressure observed in the same way.

If testing at pressures above 15 psia were desired, the vacuum pump had to be protected. A steady pressure of 15 psia was dialed in, and then the atmosphere vent valve was open. The pump was then turned off, and the pump cutoff valve was closed. The mass flow rate was then adjusted as needed.

Once testing was concluded, first the flow controller power supply was turned down such that no flow was coming through the flow controller. The vacuum pump was then turned off if testing was done on pressures below 15 psia. The atmosphere vent valve was open, if needed, to allow the cavity to reach atmospheric pressure. Finally, the helium tank was sealed.

4.2.2 Cold Flow Procedure with Ammonia as Propellant

Cold flow tests were performed with ammonia as propellant in order to establish the cavity pressures that corresponded to the available range of propellant mass flow rates. These tests were also done to compare the performance of ammonia and helium propellants.

Before the start of the test, the atmosphere vent valve had to be closed and the vacuum cutoff valve had to be opened. The helium and ammonia flow controller cutoff valves both had to be closed. Both the helium and ammonia tanks had to be opened and their regulators set to 60 psi. The vacuum pump was turned on and allowed to evacuate the system until a steady minimum pressure was reached, as indicated by the pressure transducer readout.

The system was then flushed with inert helium. This was achieved by opening the helium flow controller cutoff valve and setting the helium flow controller for around 10% of its maximum flow rate. Helium was allowed to move through the system for 30 to 60 seconds. Once the flush was complete, the helium flow was shut off and the helium cutoff valve was closed.

After the flush, to start the ammonia flow, first the ammonia flow controller cutoff valve was opened. The ammonia flow controller was then set to the desired flow rate. If the test was to take place at pressures above 15 psia, a special procedure had to be followed to protect the pump. The ammonia flow was increased until cavity pressure reached 15 psia. The atmosphere vent valve was opened, then the vacuum pump was shut off, and finally the vacuum pump shutoff valve was closed. The ammonia flow was then set to the desired rate. In all cases, once the desired rate of ammonia flow was set, the cavity pressure reading was allowed around 30 seconds to stabilize before observations were recorded.

Once the test was complete, the ammonia flow was shut off. If necessary, the atmosphere vent valve was closed, the vacuum pump cutoff valve was opened, and the vacuum pump was turned on. The ammonia cutoff valve was closed. The system was then flushed with helium again following the same procedure as before ammonia flow was started. Once the flush was complete, the helium flow was shut off, and the helium cutoff valve was closed. The vacuum pump was turned off, and the atmosphere vent valve was open to allow the system to reach atmospheric pressure. Finally, the regulator and tank valves for both helium and ammonia tanks were closed.

4.2.3 Hot Fire Procedure with Helium as Propellant

Before testing could start, the microwave power components had to be turned on and allowed to warm up. The Xicom TWTA sounds a tone when warmup is complete. The atmosphere venting valve had to be in the closed position to start testing, and the pump cutoff valve had to start in the open position. The helium tank valve had to be opened and the secondary valve reading on the regulator was set to 60 psi. Once both the microwave power and propellant systems were ready, the vacuum pump was turned on and allowed to evacuate the cavity completely.

Once the cavity pressure indicated by the pressure transducer reached a steady minimum, the helium flow was set to the desired rate and corresponding pressure using the flow controller power supply. Helium flow was allowed to continue for 30 to 60 seconds in order to minimize non-propellant gases in the cavity. While the cavity was being flushed, the desired frequency and power range was set on the HP signal generator. Once the cavity was ready, the microwave power system was engaged. The TWTA was engaged first, followed by the signal generator. The starting forward power to the cavity was set to about 5 W below expected ignition power. The power transmitted to the cavity was increased using the signal generator Vernier dial in half-watt increments, as monitored by the power sensors. About 30 seconds passed between each increase in power. This procedure continued until plasma ignition occurred. Ignition could be confirmed by a sudden change in measured forward and reflected powers and visually through the viewport.

If the experiment was expected to reach pressures above atmospheric pressure, plasma ignition was first achieved at a low pressure, and then helium flow was increased until chamber pressure reached 15 psia. At this pressure, the atmosphere vent valve was open, the pump was turned off, and then the pump shutoff valve was closed. This step was done to protect the pump since pump operation at high pressures is not recommended. With plasma ignited and the vent valve open, the helium flow could be adjusted to the desired rate.

When the experiment was complete, the signal generator was disengaged first, which extinguished the plasma. The TWTA was disengaged next, cutting off all power to the cavity. Propellant flow was turned off, followed by the vacuum pump if necessary. The atmosphere vent valve was opened to return the system to atmospheric pressure. With all systems disengaged, the equipment could be turned off if needed. Lastly, the helium tank had to be closed to conserve propellant.

4.2.4 Hot Fire Procedure with Ammonia as Propellant

Before testing, the microwave signal generator, the TWTA, and the power meters were turned on and allowed to warm up until a tone from the TWTA indicated readiness. The atmosphere vent valve was closed and the vacuum pump cutoff valve was open. Both the ammonia and helium tanks were opened and their regulators were set to 60 psi. The vacuum pump was then turned on and the system was evacuated until a steady minimum cavity pressure was reached.

The system was then flushed with inert helium. The helium cutoff valve was opened and the helium flow controller was set to about 10% of its maximum flow rate. Helium was allowed to circulate through the system for 30 to 60 seconds. Once the flush was complete, the helium flow controller was shut off and the helium cutoff valve was closed.

After the flush, the ammonia cutoff valve was opened and the ammonia flow controller was set to the desired setting. If cavity pressure had to increase above 15 psia, then upon reaching 15 psia the atmosphere vent valve was opened, the vacuum pump was turned on, and the pump cutoff valve was closed. The flow setting was then adjusted as needed. When the proper flow rate and cavity pressure were established, microwave power was engaged. The signal generator was set to the desired frequency and power ranges. The TWTA was then engaged first, followed by the signal generator. The starting forward power was set to about 5 W below expected ignition power, and then increased in half-watt increments until ignition occurred. About 30 seconds were allowed to pass between each power increase. Once ignition occurred, the necessary observations were made using the pressure transducer readout and power meters.

When the test was complete, the signal generator was disengaged first, followed by the TWTA. Ammonia flow was then turned off and the ammonia shutoff valve was closed. The system was then flushed with helium once more, using the same procedure as before ammonia flow was initiated. Once the helium flush was complete, the vacuum pump was turned off and the atmosphere vent valve was opened. If no more tests were needed in that session, all the microwave equipment was shut off. The helium and ammonia tanks and regulators were closed.

4.3 Helium Test Results

4.3.1 Helium Cold Flow Test Results

Cold flow tests were performed in order to establish the required helium flow rates to achieve a range of cavity pressures for plasma ignition and baseline performance. Microwave power was not applied in these tests. Maximum pressure inside the cavity was limited by the quartz dielectric. Results were recorded starting with a minimum observable pressure of 0.24 psia up to a maximum of 30 psia of pressure because maximum pressure calculations for the dielectric were not performed yet. This set of tests was first performed using an Omega PX303-050A5V pressure transducer. The results are shown in Figure 4.3.

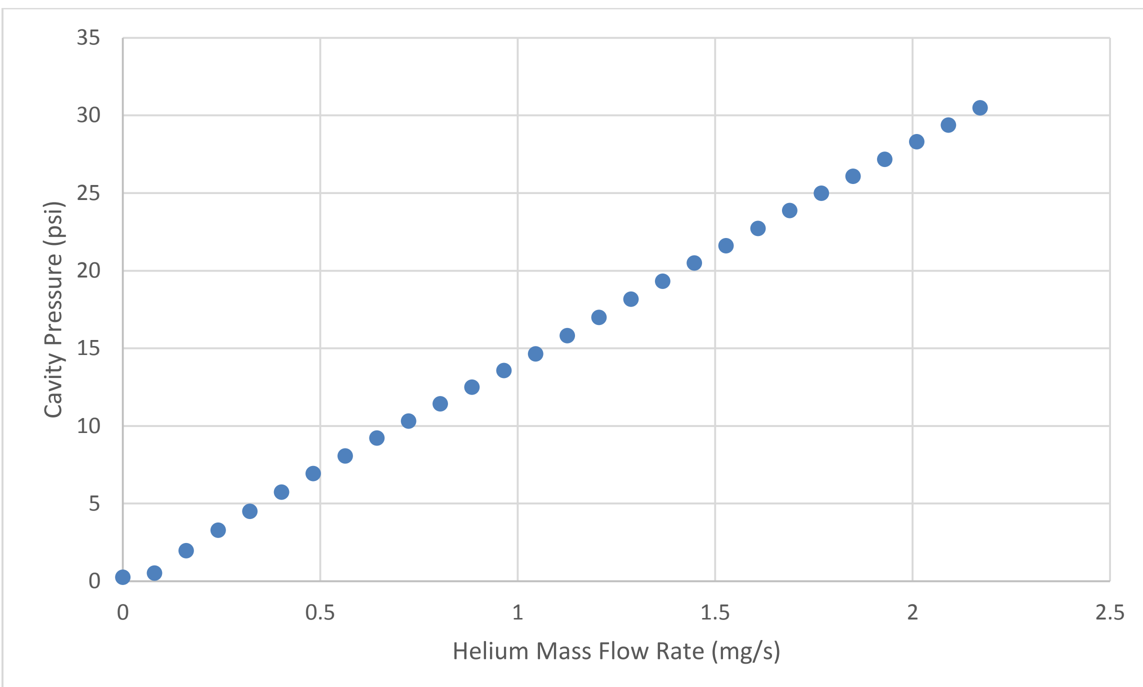

Figure 4.3: Initial cold flow cavity pressure results with helium as propellant

Pressure inside the cavity rose linearly with increasing mass flow rate of propellant. The tests were repeated after maximum pressure calculations were completed. The new set of tests were performed to a maximum pressure of 50 psia. The maximum value was determined by considering the maximum pressure that could be handled by the quartz dielectric in the thruster cavity. The calculated maximum was 47 psi above atmospheric pressure,[45] so 50 psia maximum was chosen to maintain a margin of safety. These tests were completed after the pressure transducer was changed to an Omega PX178-100S5V. Due to limitations of the equipment, data were collected from a minimum pressure of 3.15 psia, as shown in Figure 4.4.

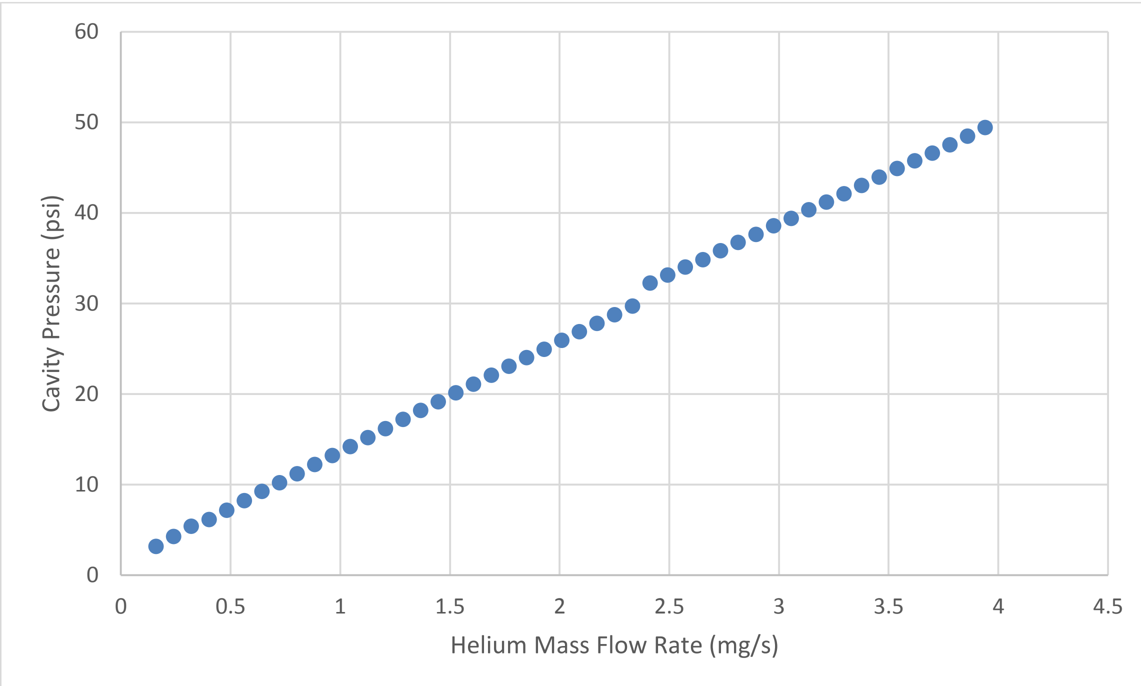

Figure 4.4: Cold flow cavity pressures with helium as propellant using updated transducer

Figure 4.4 shows that the linear increase in pressure continues all the way to the maximum operating pressure of the MET. A discontinuity can be seen in pressure values around 2.4 mg/s of flow. This was due to the opening of an atmosphere vent valve once 30 psi was reached in order to safeguard the vacuum pump, which was not meant for operation at high pressures.

Using this mass flow and pressure data, theoretical thrust values were calculated using isentropic relations. Figure 4.5 shows that 7.69 mN of thrust was the maximum at 3.94 mg/s mass flow. A small discontinuity can again be seen at 2.4 mg/s of mass flow. Figure 4.6 shows the corresponding theoretical specific impulse values.

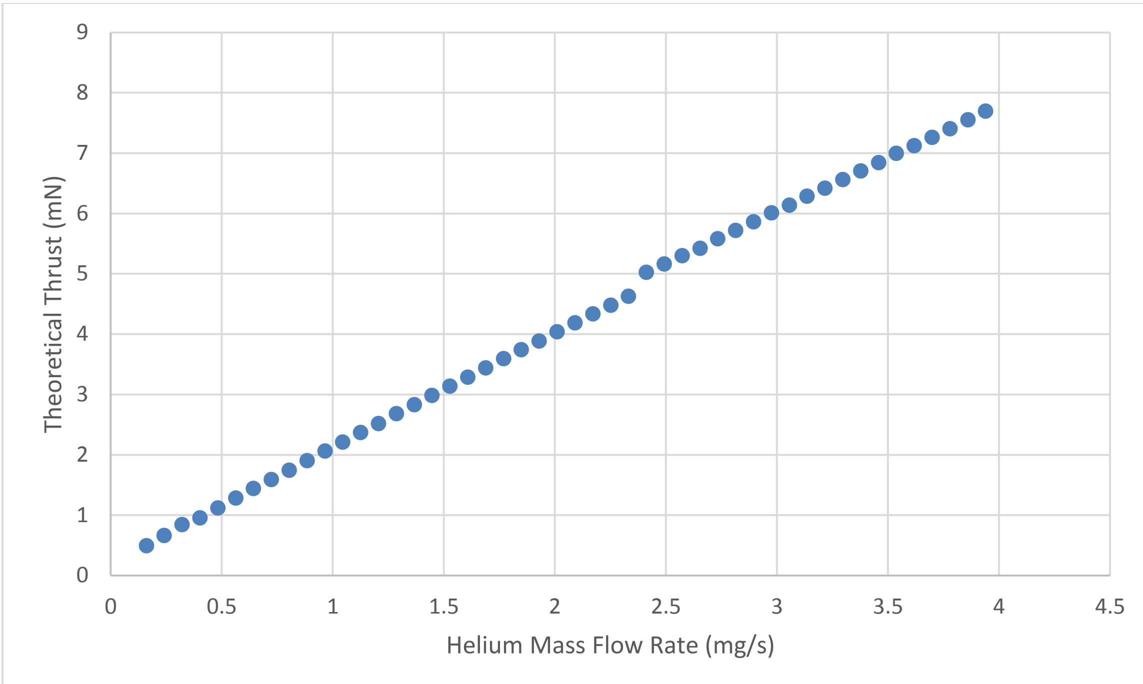

Figure 4.5: Theoretical cold flow thrust vs helium mass flow rate

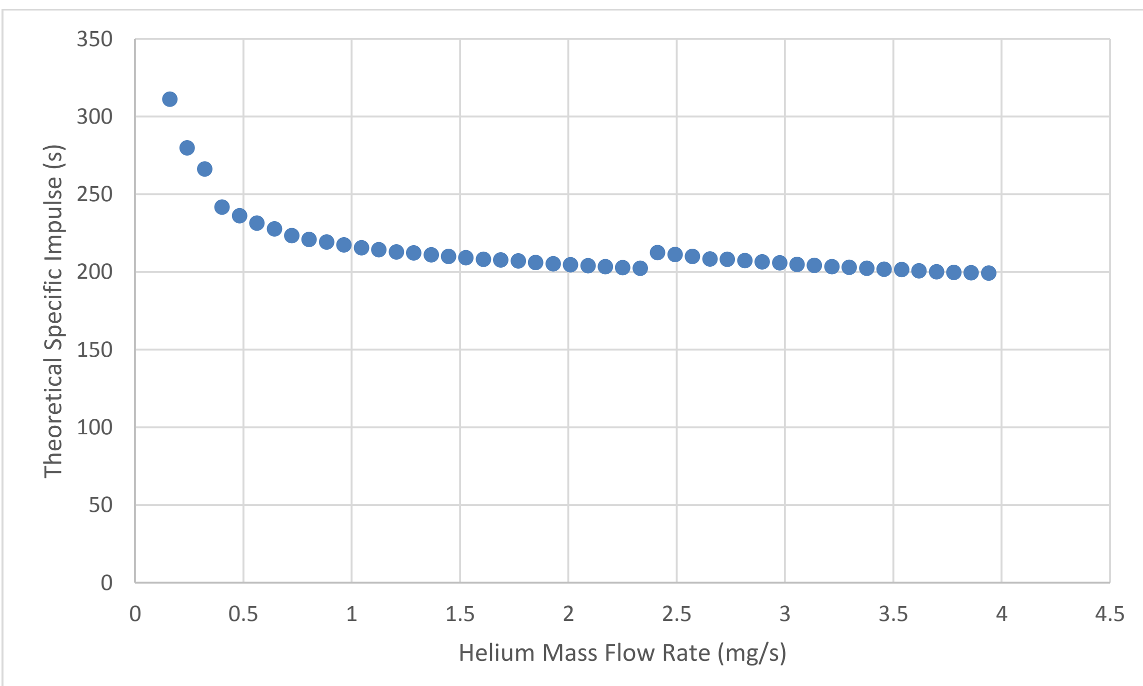

Figure 4.6: Theoretical cold flow specific impulse vs helium mass flow rate

Seen in Figure 4.6, the specific impulse started at its maximum at minimum mass propellant flow, but decreased significantly with higher mass flow values. The discontinuity at 2.4 mg/s of flow was still observed, but the decreasing trend remained the same. Overall, all specific values were low. This was expected because unheated propellant results in relatively low exit velocities, which translated to low specific impulses.

4.3.2 Helium Hot Fire Test Results

The first set of hot fire tests were performed to establish a set of plasma ignition conditions similar to a Paschen curve. Helium plasma was ignited and observed, as seen in Figure 4.7 below.

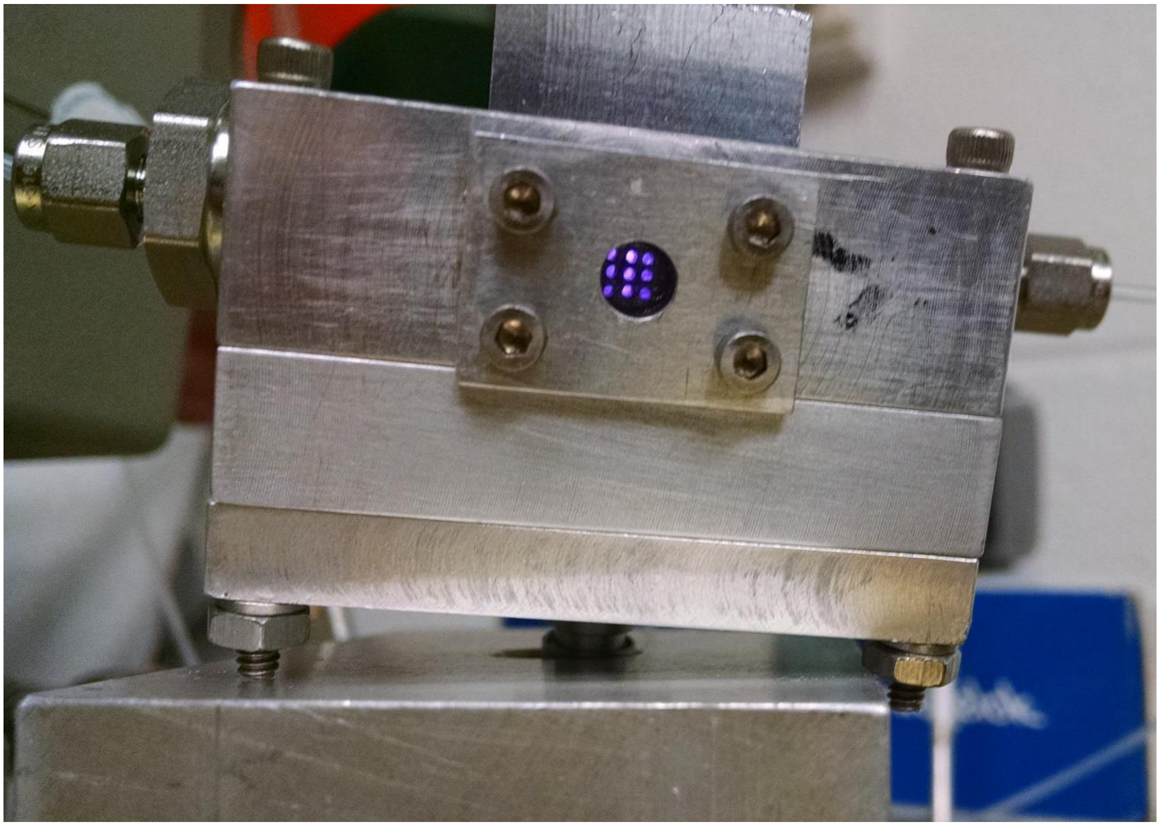

Figure 4.7: Helium plasma ignited in the MET cavity, as observed through the view port

Ignition experiments could not be completed with the original Omega PX303-050A5V transducer, so a new Omega PX178-100S5V transducer was used. The resulting data is shown in Figure 4.8.

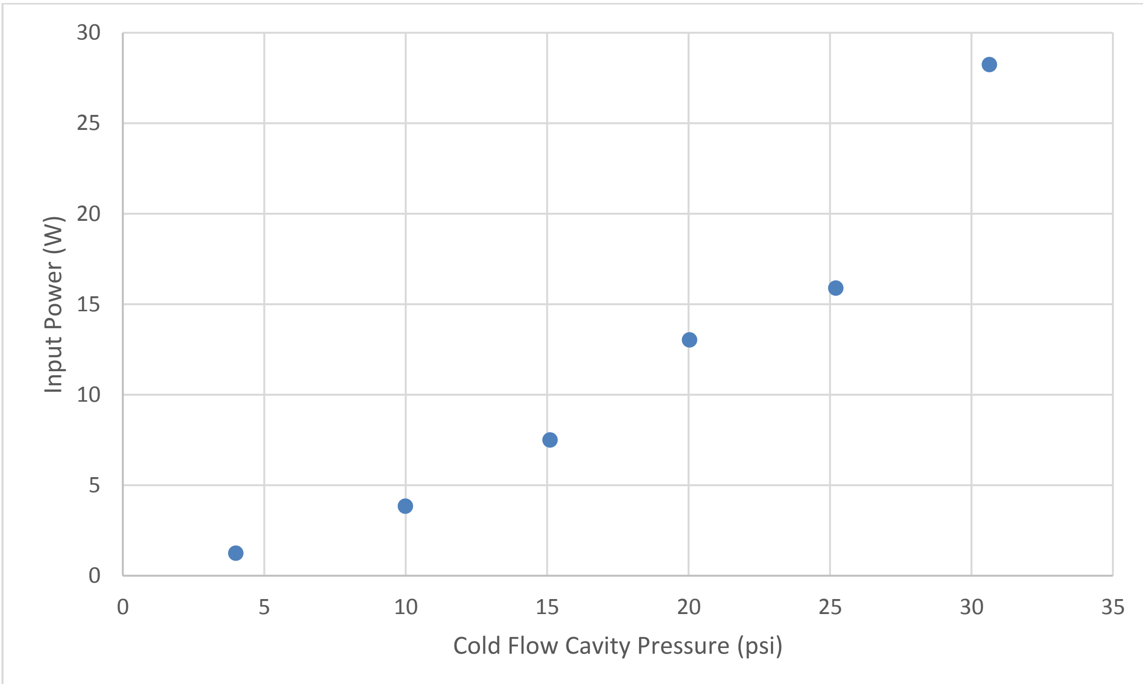

Figure 4.8: Helium plasma ignition conditions with updated pressure transducer

The ignition input power decreased with decreasing cavity pressure. Ignition power reached as low as 1.243 W at 3.99 psia. Maximum ignition power observed was 28.23 W at 30.63 psi. "Hot fire" pressure at maximum ignition power was 42.9 psia. This value approached the limit of 50 psia, so no higher ignition pressures were tested. Ignition powers even lower than 1.243 W could potentially be achieved, but lower cavity pressures could not be accurately recorded with available equipment. Power and pressure values after plasma ignition can be seen in Figure 4.9. Coupling efficiency could also be calculated using measured forward and reflected powers, and the values are shown in Figure 4.10.

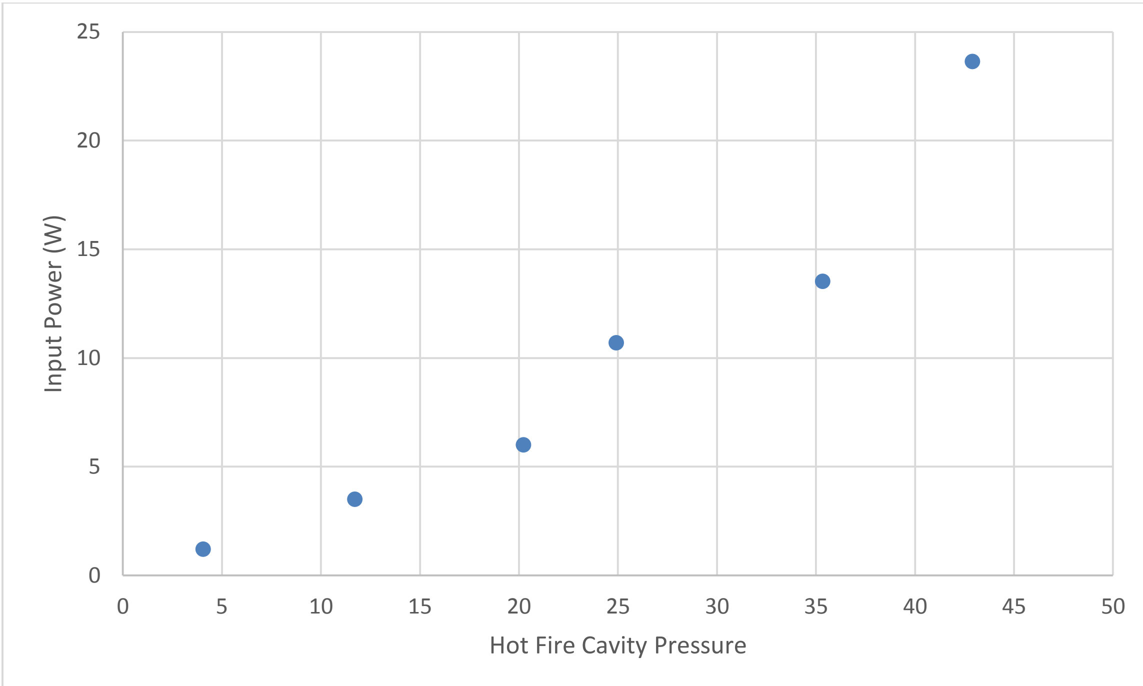

Figure 4.9: Pressure and input power conditions after helium plasma ignition

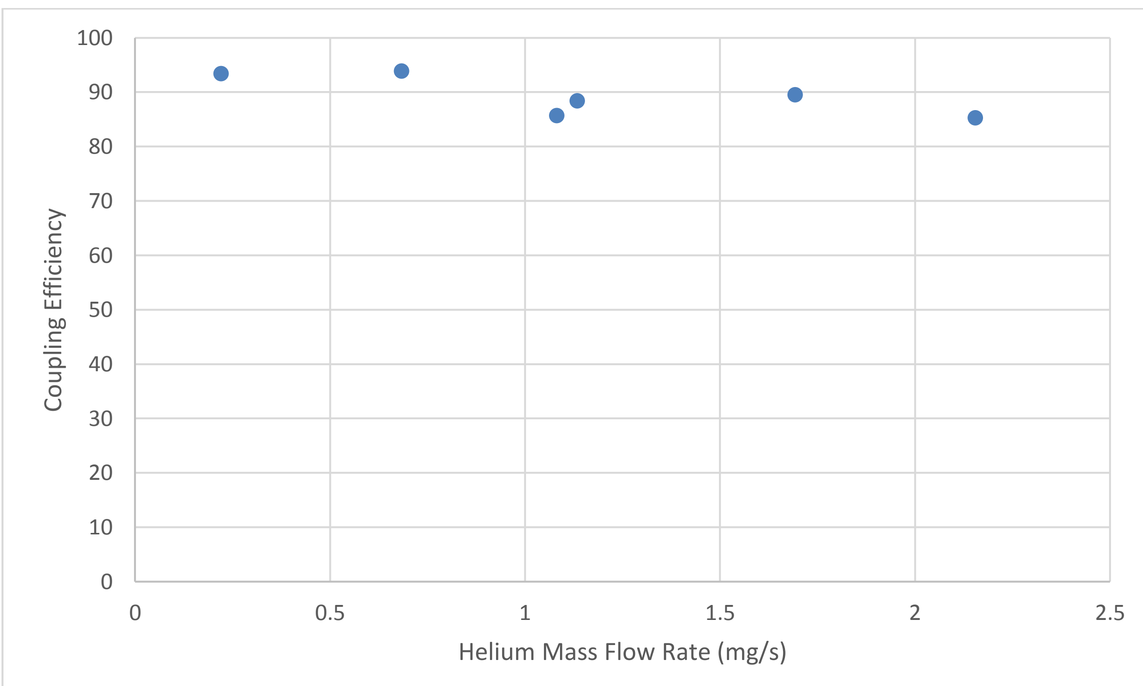

Figure 4.10: Coupling efficiency vs helium mass flow rate in the cavity

Coupling efficiency stayed relatively high, with a maximum value of 93.9% and a minimum of 85.7%. Higher coupling efficiency could likely be achieved with a better optimized antenna.

Thrust is a major factor in thruster performance. Theoretical thrust created by the MET could also be calculated from measured pressure changes using isentropic relations.

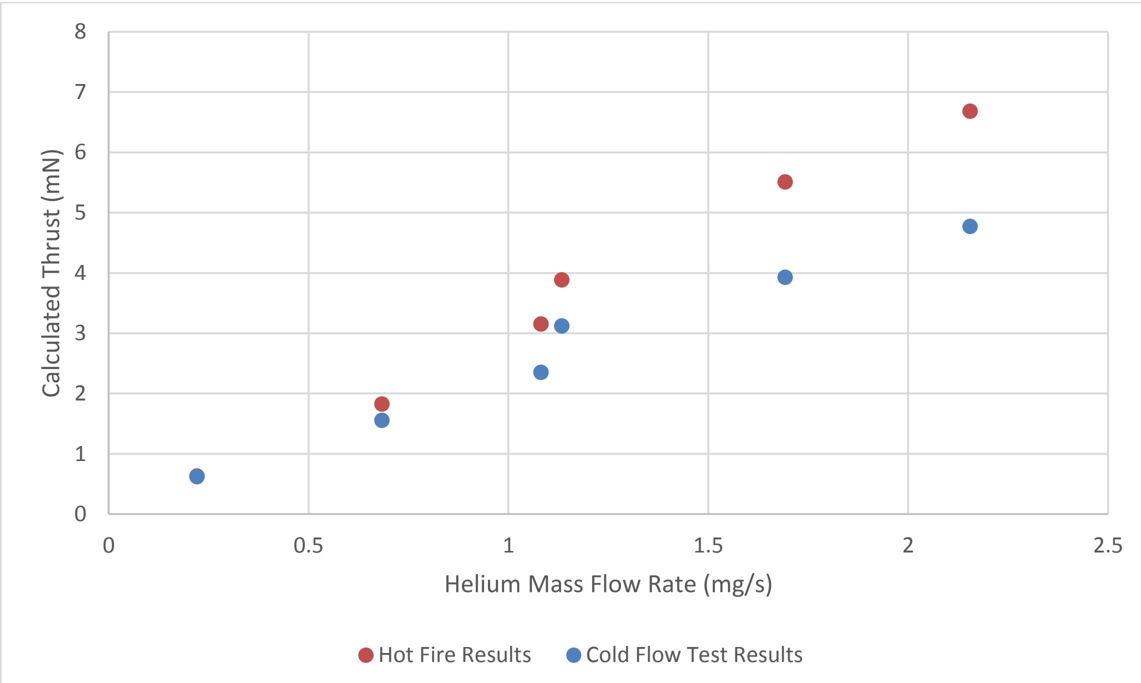

Figure 4.11: Theoretical thrust vs helium mass flow hot fire and cold flow comparison

Hot fire thrust results in Figure 4.11 show a similar pattern to the cold flow theoretical thrust from Figure 4.5. Thrust increased linearly with increasing propellant mass flow rate. Cold flow and hot fire thrusts were very similar at low flow rates, but hot fire results provided significantly higher thrusts at high propellant flow rates. Maximum theoretical thrust achieved by the thruster was 6.68 mN at a flow rate of 2.15 mg/s. There was a small discontinuity between flow rates of 1.08 mg/s and 1.13 mg/s. This was due to an atmospheric vent valve being open after cavity pressure became higher than atmospheric pressure. The valve was open to protect the vacuum pump, which was not meant to be operated at high pressures. The valve was opened at a lower pressure than during cold flow tests from the previous section.

Another common thruster performance metric is specific impulse. Theoretical specific impulse was calculated for both hot fire and cold flow results to allow a direct comparison.

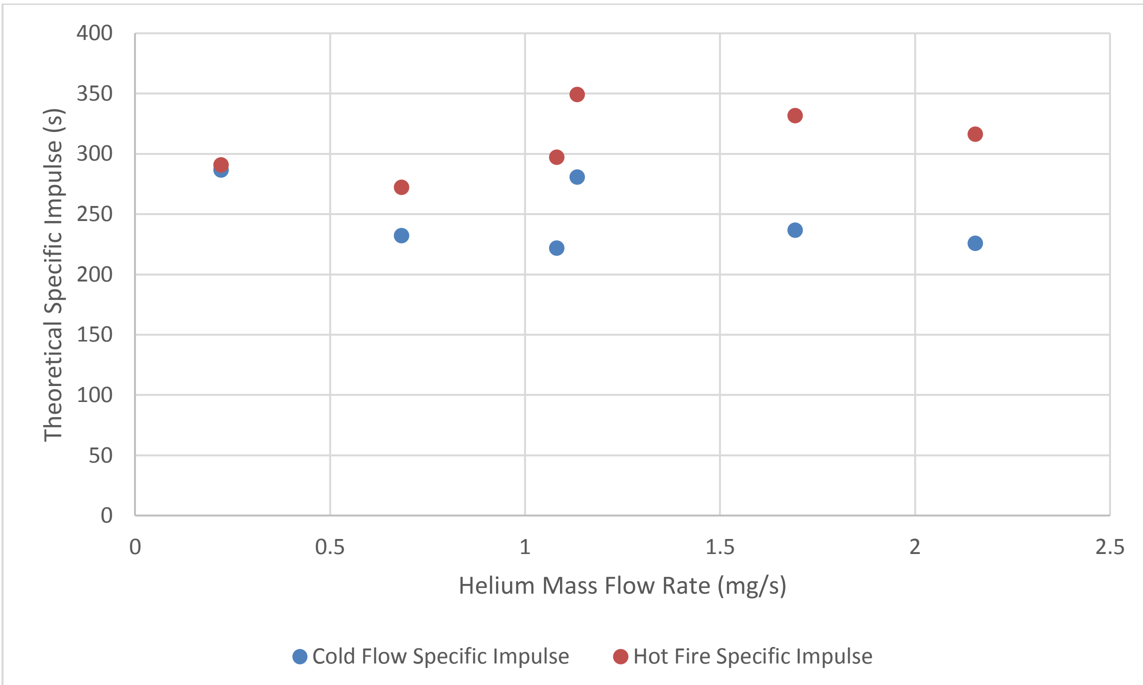

Figure 4.12: Theoretical specific impulse vs helium mass flow hot fire and cold flow comparison

Hot fire impulse was higher than cold flow specific impulse in all cases, as expected. The improvement in specific impulse becomes larger at higher flow rates. Maximum specific impulse was 349 seconds at 1.13 mg/s. The discontinuity caused by the atmosphere vent valve was present in this set of data as well. Specific impulse tended to increase in the midrange of propellant mass flow, and decreased at the low and high flow ranges.

4.4 Ammonia Test Results

Cold flow tests using ammonia were to be conducted to establish the required flow rates for a range of corresponding cavity pressures and a baseline for performance, similarly to the helium cold flow tests. After this, hot fire tests were to be performed to allow direct comparison with helium results as well. However, after the setup was completed, it was discovered that the ammonia cylinder was contaminated with water and rust. The contamination prevented collection of accurate results and plasma ignition.

Chapter 5

Conclusions and Future Work

5.1 Conclusions

The goal of this project was to design and perform a preliminary set of tests on a K_u-band, CubeSat-scale microwave electrothermal thruster. A test cavity was designed and fabricated for operation using microwave power at 17.8 GHz. Two experimental setups were assembled to gather data on plasma ignition using both helium and ammonia propellants.

After the setup was completed, plasma was successfully ignited in the cavity using helium propellant. Plasma ignition was achieved at powers as low as 1.24 W. Theoretical thrust was calculated from gathered pressure data. Maximum thrust of 6.68 mN was achieved at cavity pressure of 42.9 psi and 23.6 W of input power. Theoretical specific impulse was also calculated. A maximum of 349 seconds was achieved, with a lot of room left for improvement. Plasma ignition tests with ammonia propellant were delayed due to issues with the ammonia supplies.

5.2 Future Work

The 17.8-GHz MET is in its early stages of development, so there is a lot of work remaining until a space-ready version is produced. The current thruster version must be tested using ammonia propellant, since this is the propellant that will be used in the final version. The ammonia setup was assembled as part of this project, so this can be accomplished in the very near future.

Some components of the thruster head itself can be modified for better performance. The current nozzle is a simple one, with no converging or diverging sections. This was done for ease of manufacture, but a significant amount of optimization and improvement can be done to this part. In addition, the antenna currently used in the MET could be better optimized. Thorough experimentation with 2.4-mm candlestick antennas can be prohibitively expensive, but using optimization experience from this project, a better antenna should be constructed in the future.

Additional work after this can be done to directly measure thrust in order to compare with current theoretical values. Similarly to previous work done on other versions of the MET, a thrust stand would need to be constructed and testing would need to take place inside a vacuum chamber.

With a large amount of data gathered from this preliminary version of the thruster head, a more flight-ready MET can be designed. This would include removing excess material around the cylindrical cavity, optimizing material selection for best electromagnetic properties, and streamlining the propellant ports. Additional work on the dielectric insert might be done as well, since quartz glass might be too fragile for a flight model.

Work should also be done on a tabletop model of the whole CubeSat thruster module. Design work and part selection for the microwave source, propellant tank, valve systems, and propellant delivery systems are all in very early stages as well.

References

1. Hill, Philip G., and Carl R. Peterson, *Mechanics and Thermodynamics of Propulsion*, 2nd Edition, Reading, MA: Addison-Wesley, 1992.

2. Micci, M. M., S. G. Bilén, and D. E. Clemens. "History and Current Status of the Microwave Electrothermal Thruster." *Progress in Propulsion Physics 1 (2009): 425-38 [online publication]*. URL: http://www.eucass-proceedings.eu/index.php?option=com_article&access=doi&doi=10.1051/eucass/200901425&Itemid=129.

3. Adusumilli, Rohit P., "*Performance Evaluation and Optimization of High Power 14.5 GHz Miniature Microwave Electrothermal Thruster,*" Master of Science Thesis, The Pennsylvania State University, 2011.

4. Balaam, P., Maul, W., and Micci, M. M., "*Characteristics of Free Floating Nitrogen and Helium Plasmas Generated in a Microwave Resonant Cavity*," IEPC-88-099, 20th DGLR AIAA JSASS International Electric Propulsion Conference, Garmisch Partenkirchen, W. Germany, Oct 1988.

5. Sullivan, Daniel J., "*Development and Performance Characterization of a Microwave Electrothermal Thruster Prototype*," Doctor of Philosophy Dissertation, The Pennsylvania State University, 1995.

6. Kline, J.F., "*Thrust Measurements of a Microwave Electrothermal Thruster,*" Master of Science Thesis, The Pennsylvania State University, 1996.

7. Nordling, David, A., "*High-Frequency Low-Power Microwave Arcjet Thruster Development,*" Master of Science Thesis, The Pennsylvania State University, 1998.

8. Souliez, F.J., "*Low-Power Microwave Arcjet Spectroscopic Diagnostics and Performance Evaluation,*" Master of Science Thesis, The Pennsylvania State University, 1999.

9. Roos, Carl, J. A., "*Vertical-Deflection Thrust Stand Measurements of a Low Power Microwave Arcjet Thruster,*" Master of Science Thesis, The Pennsylvania State University, 2001.

10. Welander, Benjamin, A., "*Low Power Microwave Arcjet Thruster Using Nitrogen Propellant,*" Master of Science Thesis, The Pennsylvania State University, 2004.

11. Clemens, Daniel, E., "*Performance Evaluation of a Low-Power Microwave Electrothermal Thruster,*" Master of Science Thesis, The Pennsylvania State University, 2004.

12. Clemens, Daniel, E., "*Performance Evaluation of the Microwave Electrothermal Thruster Using Nitrogen, Simulated Hydrazine, and Ammonia,*" Doctor of Philosophy Dissertation, The Pennsylvania State University, 2008.

13. Blum, Jacob H., "*Performance Evaluation and Optimization of an 8-GHz Microwave Electrothermal Thruster,*" Master of Science Thesis, The Pennsylvania State University, 2009.

14. Hopkins, Jeffrey, R., "*Design Optimization and Direct Thrust Measurement of an 8-GHz Microwave Electrothermal Thruster,*" Master of Science Thesis, The Pennsylvania State University, 2011.

15. Goovaerts, Karl, M., "*Feasibility Studies of a 14.5-GHz, Low Power Microwave Electrothermal Thruster,*" Master of Science Thesis, The Pennsylvania State University, 2007.

16. Adusumilli, Rohit, P., "*Performance Evaluation and Optimization of High-Power 14.5-GHz Miniature Microwave Electrothermal thruster,*" Master of Science Thesis, The Pennsylvania State University, 2011.

17. Capalungan, Erica, E., "*Design and Development of a 30-GHz Microwave Electrothermal Thruster,*" Master of Science Thesis, The Pennsylvania State University, 2011.

18. Balanis, Constantine, A., *Advanced Engineering Electromagnetics,* 2nd Edition, John Wiley & Sons, Inc., 2012.

19. Harrington, Roger F., *Time-Harmonic Electromagnetic Fields,* IEEE Press, 2011.

20. Chen, Francis, F., *Introduction to Plasma Physics and Conrolled Fusion,* 2nd Edition, Plenum Press, 1984.

21. Raizer, Yuri P., *Gas Discharge Physics,* Springer-Verlag Berlin Heidelberg, 1991.

22. Mission Design Division Staff, NASA, "*Small Spacecraft Technology State of the Art*," July 2014.

23. "About Us," *CubeSat*, URL: http://www.cubesat.org/index.php/about-us.

24. Shiroma, Wayne A. et al., "CubeSats: A Bright Future for Nanosatellites," *Central European Journal of Engineering [online publication]*, 2011, URL: http://link.springer.com.ezaccess.libraries.psu.edu/article/10.2478%2Fs13531-011-0007-8.

25. Selva, Daniel, Krejci, David, "A Survey and Assessment of the Capabilities of CubeSats for Earth Observation," *Acta Astronautica*, Vol 74, May-June 2012, pp. 50-68, URL: http://www.sciencedirect.com/science/article/pii/S0094576511003742.

26. Nugent, Ryan, Munakata, Riki, et al., "*The CubeSat: The Picosatellite Standard for Research and Education,*" Aerospace Engineering Department, California Polytechnic State University, 2008, URL: http://cubesat.org/images/More_Papers/cps2008.pdf.

27. "Dnepr UniSat-6 Launch 2014," *CubeSat*, URL: http://cubesat.org/index.php/missions/past-launches/142-dnepr-unisat-6-launch-2014.

28. Sarda, K., Grant, C., Eagleson, S., Kekez, D., Zee, R., "*Canadian Advanced Nanosatellite Experience 2 Orbit Operations: Two Years of Pushing the Nanosatellite Envelope,*" in: Proceedings of the 61st International Astronautical Congress, 2010.

29. "CanX-4&5 Formation Flying Mission Accomplished," *University of Toronto Institute for Aerospace Studies Space Flight Laboratory*, URL: utias-sfl.net/?p=2191.

30. "Delfi-n3Xt Micropropulsion Payload," *Delfi Space,*URL: www.delfispace.nl/delfi-n3xt/micropropulsion-payload.

31. Parker, J.M., Thunnissen, D., Blandino, J., and Ganapathi, G., "*The Preliminary Design and Status of a Hydrazine MilliNewton Thruster Development,*" AIAA Paper 99-2596, 35th AIAA/ASME/SAE/ASEE Joint Propulsion Conference, June 20-24, Los Angeles, CA, 1999.

32. Mueller, J., Hofer, R., Ziemer, J., "*Survey of Propulsion Technologies Applicable to CubeSats,*" Jet Propulsion Laboratory, California Institute of Technology, Pasadena, CA, 2010.

33. Kvell, U., Puusepp, M., Kaminski, F., Past, J., Palmer, K., et al, "*Nanosatellite orbit control using MEMS Cold Gas Thrusters,*" Proceedings of the Estonian Academy of Sciences, 2014.

34. Müller, C., Lebbink, L., Zandbergen, B., Brouwer, G., Amini, R., Kajon, D., Sanders, B., "Implementation of the $T^3\mu PS$ in the Delfi-n3Xt Satellite," book selection, *Small Satellite Mission for Earth Observation,* 2010, pp 411-424.

35. Goldberg, Hannah, Mueller, Juergen, Alkalai, Leon, "*Micro-Inspector Spacecraft: An Overview,*" presented at 20th Annual AIAA/USU Conference on Small Satellites, 2006.

36. "*Micro Propulsion Systems,*" VACCO Industries, URL: www.vacco.com/images/uploads/pdfs/MicroPropulsionSystems.pdf.

37. "*HYDROS Thruster Product Sheet,*" Tethers Unlimited, Inc., URL: www.tethers.com/SpecSheets/Brochure_HYDROS.pdf.

38. "*Micro Pulsed Plasma Thruster,*" Busek Space Propulsion and Systems Co, Inc., URL: www.busek.com/index_htm_files/70008502E.pdf.

39. Kronhaus, I., Schilling, K., Jayakumar, S., Kramer, A., "*Design of the UWE-4 Picosatellite Orbit Control System using Vacuumo-Arc-Thrusters,*" presented at 33rd International Electric Propulsion Conference, 2013.

40. Taunay, Pierre-Yves, "*Testing and Optimization of a Miniature Microwave Ion Thruster,*" Master of Science Thesis, The Pennsylvania State University, 2012.

41. "*Busek Electrospray Thrusters,*" Busek Space Propulsion and Systems Co, Inc., URL: www.busek.com/index_htm_files/70008500F.pdf.

42. "*Busek Micro Resistojet,*" Busek Space Propulsion and Systems Co., Inc., URL: www.busek.com/index_htm_files/70008518B.pdf.

43. Sinha, Swarna, "*Numerical Modeling of a 17.8 GHz Microwave Electrothermal Thruster,*" Undergraduate Honors Thesis, The Pennsylvania State University, 2013.

44. Abaimov, Mikhail, "*Design of a Microwave Electrothermal Thruster Module for Use on a CubeSat Platform*," Undergraduate Engineering Science Thesis, The Pennsylvania State University, 2013.

45. "*Pressure Determination of Fuzed Quartz,*" Momentive Performance Materials, Inc., URL: http://www.momentive.com/products/main.aspx?id=20350.